Probing the Surface Chemistry of Self-Assembled Peptide Hydrogels using Solution-State NMR Spectroscopy

Matthew Wallace,[a,*] Jonathan A. Iggo[a] and Dave J. Adams[a,b,*]

[a] *Department of Chemistry, University of Liverpool, Crown Street, Liverpool, L69 7ZD, U.K. Email: dave.adams@glasgow.ac.uk*

[b] *Current address: School of Chemistry, College of Science and Engineering, University of Glasgow, Glasgow, G12 8QQ, U.K.*

Electronic Supplementary Information (ESI)

1. Effect of added probe molecules/ions on gelation

As in our previous work,[1] we assess the effect of our probe molecules and ions on the gelation process by systematically excluding certain probes and observing those that remain. If the RQCs, STDs and ^{23}Na relaxation times follow the same pattern in the absence of a probe then we can be confident that the probe does not significantly affect the formation of the gel; the surface chemistry, kinetics of gel formation and anisotropy of the fibres with respect to the spectrometer magnetic field are the same in its presence/absence.

1.1. Effect of added probe molecules on the formation of **1**/GdL gels

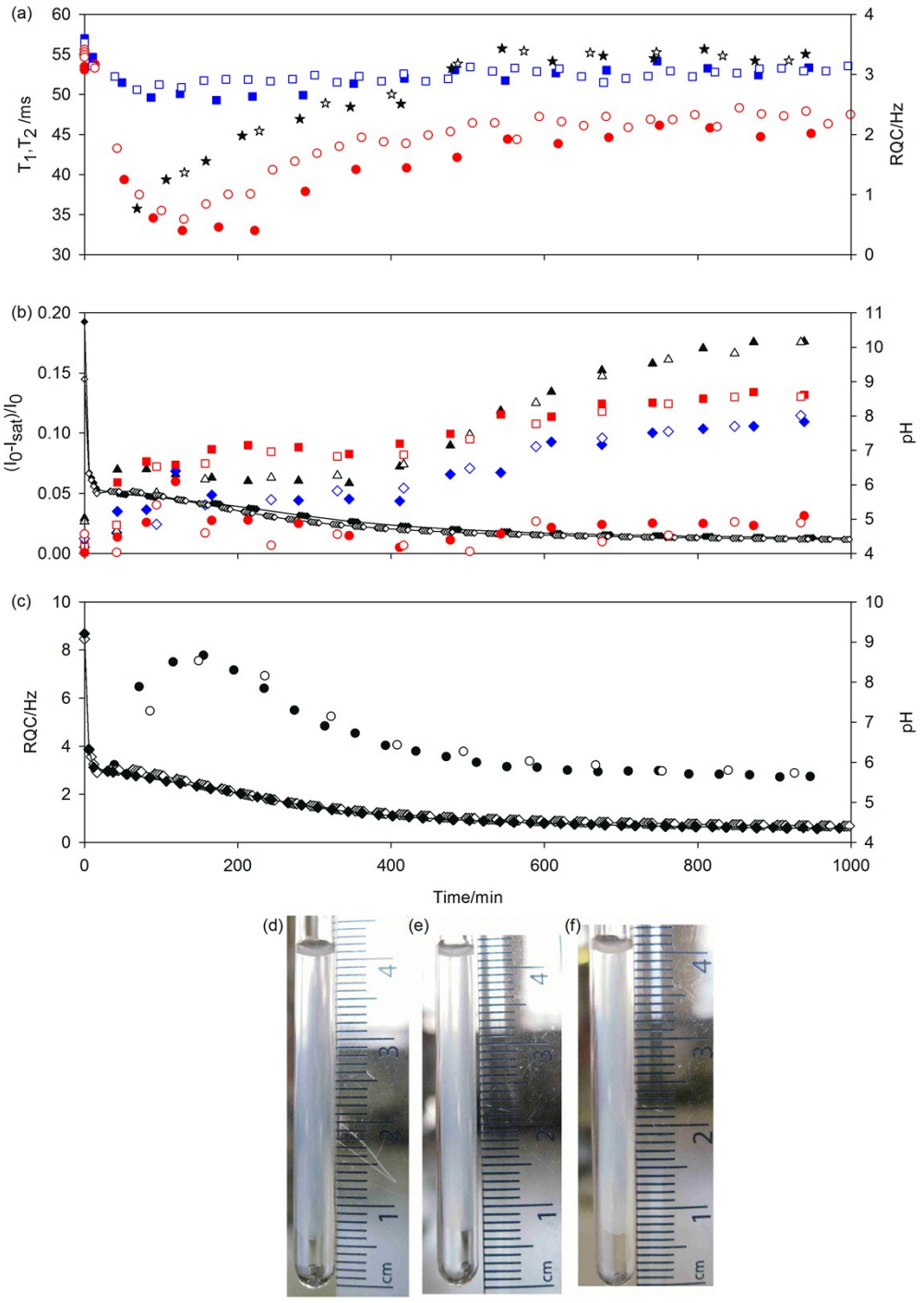

Figure S1a. Plots of experimental observables during formation of **1**/GdL hydrogels containing all (hollow) or part (solid) of the standard set of probe molecules. (a) Plot of ^{23}Na T_1 (blue square), T_2 (red circle) and IPA RQC (black star). Solid shapes correspond to sample containing no NH_4Cl, sodium formate-d or ^2H organic solvents other than IPA. (b) Plots of STDs to acetone (black triangle), IPA (blue diamond), tBuOH (red square) and $MeNH_3^+$ (red circle). The pH (black diamond) is also plotted. The lines are a guide to the eye. Solid shapes correspond to the same sample as (a). (c) Plot of $^{14}NH_4^+$ RQC (circle) and pH (diamond). Solid shapes correspond to sample containing 10 mM NH_4Cl and no organic solvents, $MeNH_3Cl$ or formate-d. Photographs of gel samples containing the full set of probes (d), 10 mM NH_4Cl and no ^2H organic solvents, formate-d or $MeNH_3Cl$ (e) and no NH_4Cl, formate-d or ^2H organic solvents other than IPA (f).

In the absence of NH_4Cl, sodium formate-d or ^2H solvents other than IPA, the RQCs (a) and STDs (b) of the remaining probe molecules follow the same profiles as in their presence, implying a near identical surface chemistry and gelation kinetics. The apparent lack of competition between IPA and the other solvents for the fibres implies that these probes interact only weakly with the fibres, with the majority of surface binding sites being unoccupied. The slight difference in the profiles of the ^{23}Na T_2 relaxation time (a) can be ascribed to competition between NH_4^+ and Na^+ for the negative charge of the fibres. A more dramatic competition effect is observed on the $^{14}NH_4^+$ RQCs when 5 mM benzylammonium (**D1**) is included in addition to NH_4Cl (Section 5.1) or on the $^{23}Na^+$ T_1 relaxation time in solutions of **2** in the complete absence of additional probe cations (Section 1.2). In the absence of all organic solvents, formate-d and $MeNH_3Cl$, the $^{14}NH_4^+$ RQC (c) follows much the same profile as in the presence of these probes, again implying a near identical surface chemistry. The slightly faster kinetics of gel formation in the absence of the probes can be ascribed to differences in the weighing of the GdL and the effect of 5 mM formate-d on the hydrolysis of GdL and the pH of the sample.[2, 3] As described in our previous work,[1] a faster decrease in the pH results in faster gelation kinetics. Accordingly, when the non-assembling propionic acid is included in the place of **1**, the pH profiles are slightly different in the two probe mixtures (Figure S1b), with the basic formate-d giving a slightly raised pH curve. All samples synerese to very similar extents (e-f).

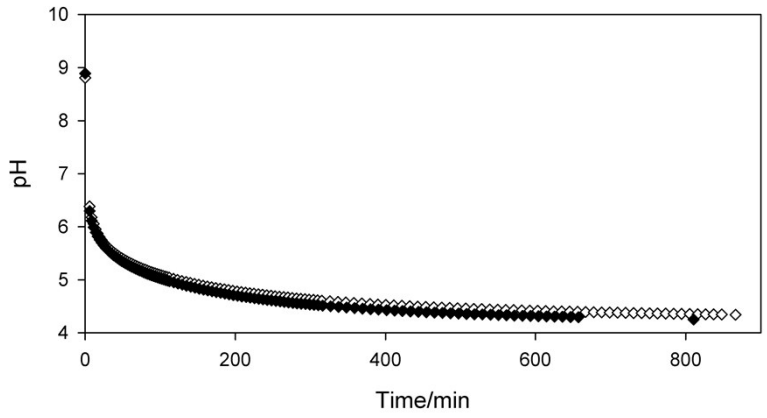

Figure S1b. Plot of pH versus time following the addition of 5 mg/mL GdL to solutions containing propionic acid in place of **1**. Solutions contained the full set of probes used for **1**/GdL samples (white) or with no organic solvents, $MeNH_3Cl$ or formate-d (black).

The integrals of the probe molecules remain constant throughout the experiment (Figure S1c) confirming minimal inclusion of the probes in the fibres. The NMR resonances of the probes also remain sharp (Figure S5b), again consistent with the probes remaining in the solution phase of the gel. Overall, we can be confident that the set of probe molecules/ions used for **1**/GdL gels does not significantly affect the formation of the gel or the observed surface chemical properties. Further plots are presented in our previous work.[1]

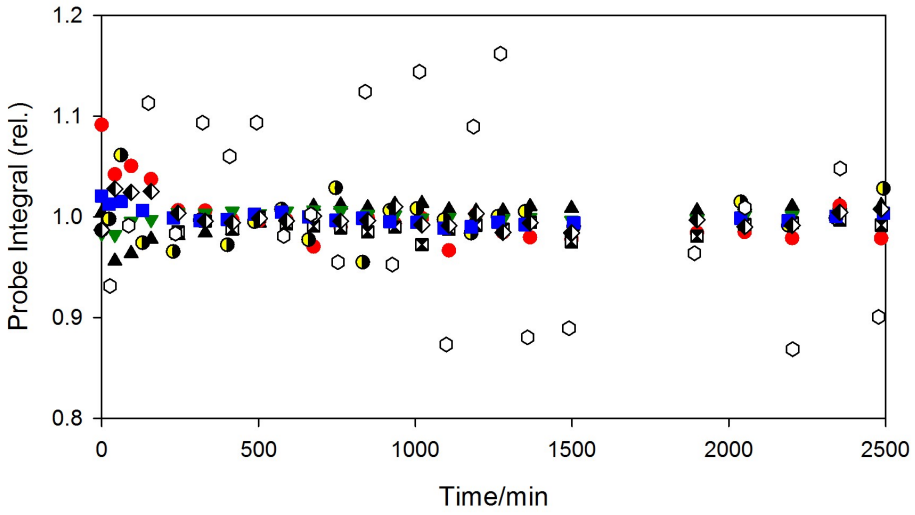

Figure S1c. Plot of NMR integrals of probe molecules versus time during gelation of a **1**/GdL sample: IPA+tBuOH (blue square), acetone (black triangle), $MeNH_3^+$ (red circle), DMSO (green down triangle), formate (half black circle), acetate (black and white square), MeOH (black and white diamond) and $^{14}NH_4^+$ (white hexagon). Integrals have been normalised to the average value recorded in the time series. The ^2H resonances of IPA, tBuOH and formate are plotted instead of the ^1H integrals owing to a slight overlap of their ^1H integrals with those of **1**.

1.2. Effect of added probe molecules on **2**/$CaCl_2$ gels

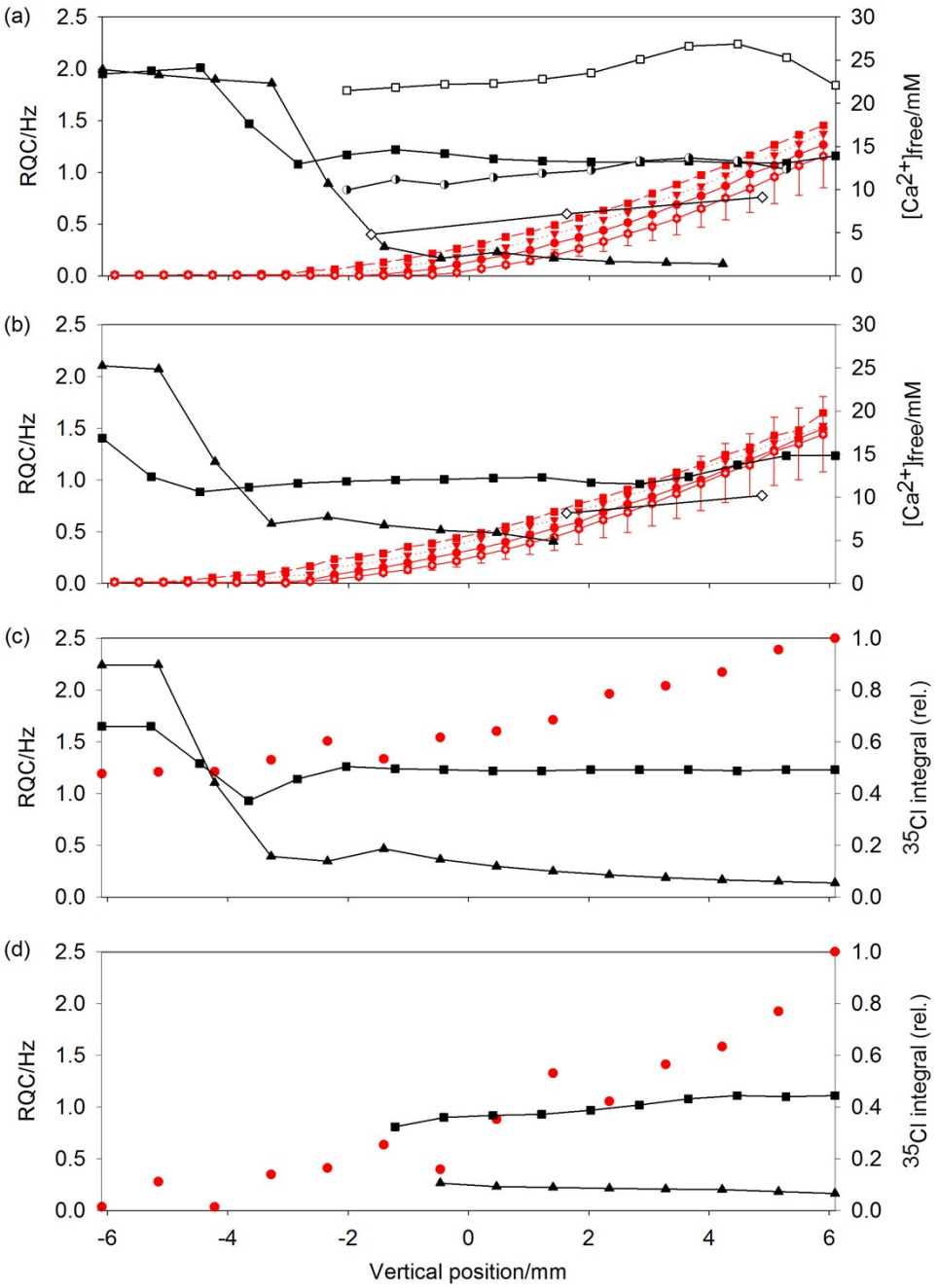

Figure S1d. Plots of experimental observables along length of **2**/$CaCl_2$ gel samples during gelation. Samples were prepared with different sets of probe molecules: (a) full set of probes for **2**/$CaCl_2$ gels (Figure 5) reproduced here for convenience, (b) full set but with organic solvents excluded, (c) all probes excluded but with 30 mM NaCl added in their place, (d) no probe molecules. RQCs: $^{23}Na^+$ (black triangle), formate-d (white diamond), HDO (black square), dioxane (white square) and tBuOH (half-black circle). In all plots, the $^{23}Na^+$ RQC has been scaled down by a factor of 500. Only resolvable RQCs are plotted. Red: Profiles of $[Ca^{2+}]_{free}$ before all images (hollow hexagon) – error bars indicate uncertainty in $[Ca^{2+}]_{free}$ measurements – after ^{23}Na image (circle), after formate-d image (down triangle) and after ^2H HDO, tBuOH and dioxane image (square). The lines are a guide to the eye. In samples where maleate was excluded (c, d), the integral of the $^{35}Cl^-$ resonance (red circle) is plotted instead of $[Ca^{2+}]_{free}$, recorded after the ^{23}Na and ^2H images.

The standard set of probes used for **2**/$CaCl_2$ gels includes 30 mM of ionic compounds as well as organic solvents. Such a high concentration of ions is necessary due to the low sensitivity of CSI methods compared to conventional NMR. However, it is apparent from Figure S1d (a, c) that inclusion of the full set of probes has much the same effect on the samples as inclusion of 30 mM NaCl, the HDO and $^{23}Na^+$ RQCs following very similar profiles.

In the absence of all probe molecules, ions and $CaCl_2$, the solutions of **2** do not display any birefringent domains[4] (Figure S1e) while no RQCs of HDO or $^{23}Na^+$ are observable (Figure S1d, d). The $^{23}Na^+$ RQC is not observable due to the very strong interaction of Na^+ with the structures of **2** in the absence of excess Na^+; the $^{23}Na^+$ T_1 in this solution was measured as 26±1 ms compared to 41±1 ms in a solution with the full set of probes, confirming a stronger interaction. Upon addition of $CaCl_2$, RQCs of HDO and $^{23}Na^+$ become apparent (Figure S1d, d) while the $^{23}Na^+$ T_1 in the final gel is measured as 55±1 ms. These results are consistent with a displacement of Na^+ from the structures of **2** by the Ca^{2+}. It can also be observed that following initial binding of Ca^{2+} (0 mm, Figure S1d, d), the HDO RQC remains essentially invariant as more $CaCl_2$ diffuses down the tube. Even in the complete absence of probes, the formation of **2**/$CaCl_2$ gels is thus fundamentally similar to their formation in the presence of the full set of probes: Ca^{2+} displaces Na^+ from the structures which soon become saturated with Ca^{2+}, the addition of more $CaCl_2$ having little effect on the observable properties of the samples.

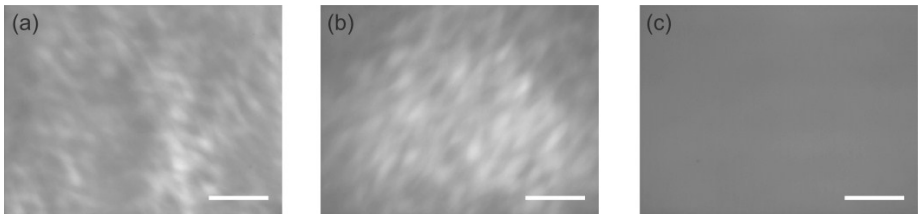

Figure S1e. Optical images of 4 mg/mL solutions of **2** at pH 9 recorded between crossed-polarisers. (a) Full set of probes included, (b) 30 mM NaCl in place of all probes, (c) No probes. The scale bars represent 0.5 mm. Images were recorded in transmission mode on a Nikon Eclipse LV100POL under X5 magnification between crossed-polarised filters. The samples were contained in 5 mm NMR tubes mounted on glass slides. Following preparation, the samples were aged for seven days before analysis. Upon addition of $CaCl_2$, the birefringence of (a) and (b) is lost which is likely due to a change in the hierarchical organisation of the structures of **2** (data not shown).[4]

^{35}Cl CSI experiments (Figure S1d) were performed using the same pulse sequence used for ^2H CSI experiments with 32 gradient steps. 626 data points were acquired with a sweep width of 10 ppm and a signal acquisition time of 0.2 s. The total acquisition time for the image was 45 minutes. ^{35}Cl integrals are normalised to the maximum value obtained in the NMR-active window. The theoretical spatial resolution is 0.94 mm.

We note that it is possible to double the concentration of all ^2H probes without affecting the gel (Figure S1f); the RQCs of all probes are very similar between the two samples and follow identical profiles along the Ca^{2+} gradient. By using 10 mM formate-d instead of 5 mM, the formate RQCs can be recorded with a much higher spatial resolution in the same image as the other ^2H probes (Figure S1f, b). It can now be seen that the RQC of the formate emerges after that of dioxane. A very slight excess of Ca^{2+} is thus required in order to sufficiently neutralise the negative charge of the fibres for the anionic formate to interact and exhibit an RQC. The lack of a concentration dependence of the

RQCs implies a relatively weak binding of these probes to the fibres with the majority of binding sites remaining unoccupied. The sharp ^{2}H resonances of the probes are also consistent with a weak interaction.

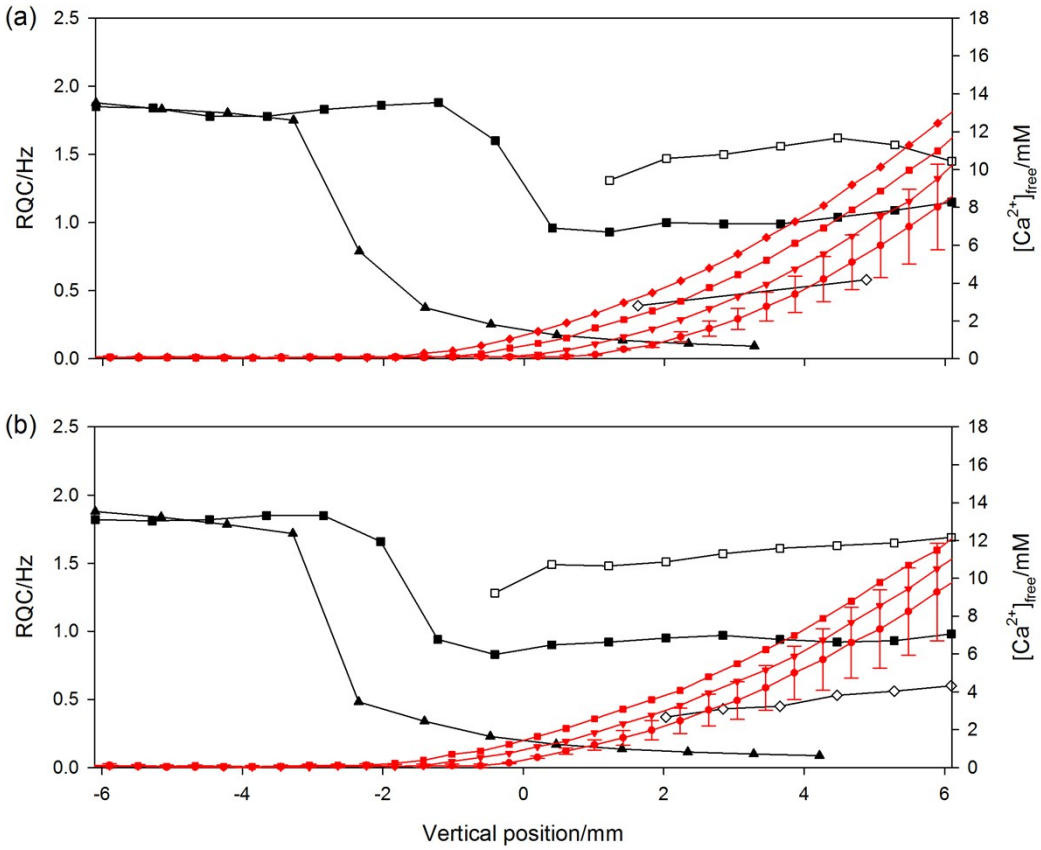

Figure S1f. Plots of experimental observables along length of an NMR sample. 0 mm corresponds to the centre of the NMR-active region. RQCs of $^{23}Na^{+}$ (triangle), HDO (black square), dioxane (white square) and formate-d (white diamond). (a) Standard set of probe molecules for **2**/$CaCl_2$ gels. $[Ca^{2+}]_{free}$ (red) before all images (circle), after ^{2}H HDO and dioxane image (triangle), after ^{2}H formate image (square) and after ^{23}Na image (diamond). (b) Standard set but with the concentration of all ^{2}H probes doubled. Only 5 mM NaCl was added to this sample so that the concentration of Na^{+} was the same in the two samples. $[Ca^{2+}]_{free}$ before all images (circle), after ^{2}H image (triangle) and after ^{23}Na image (square). In both plots, the ^{23}Na RQCs have been scaled down by a factor of 500. On these plots, the ^{23}Na image was run after the ^{2}H image, whereas for Figure 5, the ^{23}Na image was recorded before all other images.

Finally, we note that the NMR integrals of the probe molecules remain constant along the Ca^{2+} gradient implying minimal inclusion of the probes in the gel fibres (Figure S1g).

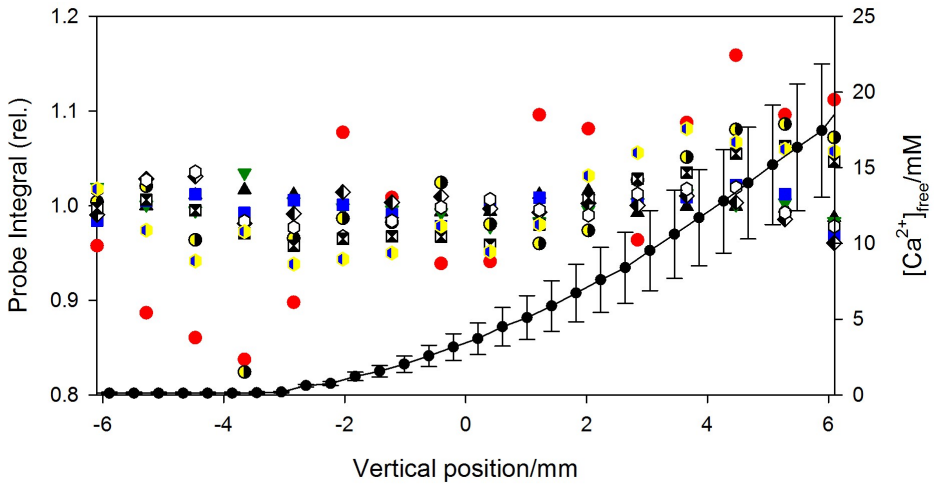

Figure S1g. Plot of ^{1}H NMR integrals of probe molecules along the length of a sample during the formation of **2**/$CaCl_2$ gel: maleate (red circle), DMSO (green down triangle), MeOH (black and white diamond), acetate (black and white square), tBuOH (blue square), MPA^{2-} (blue and yellow hexagon), formate (half black circle) and dioxane (white hexagon). $[Ca^{2+}]_{free}$ is plotted as black circles linked by a line, with the uncertainty indicated. Integrals are normalised to their average value in the series.

1.3. Effect of magnetic field during gelation

In our previous work,[1] we demonstrated that the presence of the magnetic field during gelation does not significantly affect the mechanical properties or the ^{23}Na relaxation times of **1**/GdL gels. The syneresis of the gels also occurs to a very similar extent in the presence and absence of the field. The STDs to the probe molecules are also very similar in a gel prepared away from the magnetic field, confirming that the observed surface chemistry of the gels is unaffected by the presence of the magnetic field during gelation.

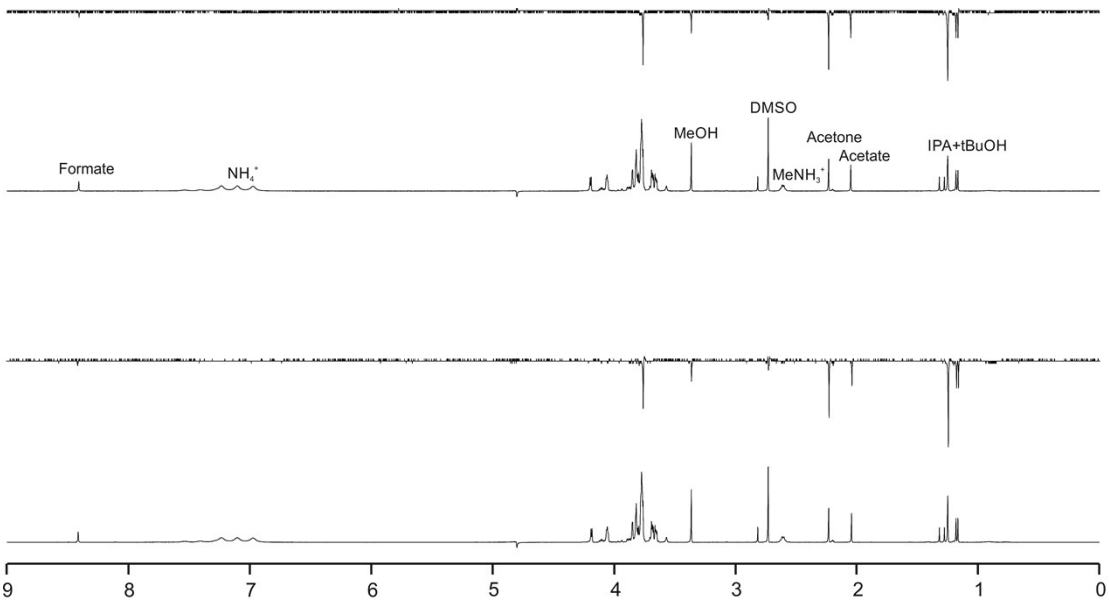

Figure S1h. ^{1}H NMR spectra of **1**/GdL gel prepared away from the magnetic field of the spectrometer (bottom) and in the field (top). The STD difference spectra (I_{sat}-I_0) are displayed above the reference ^{1}H spectra (I_0) and have been scaled by a factor of 10.

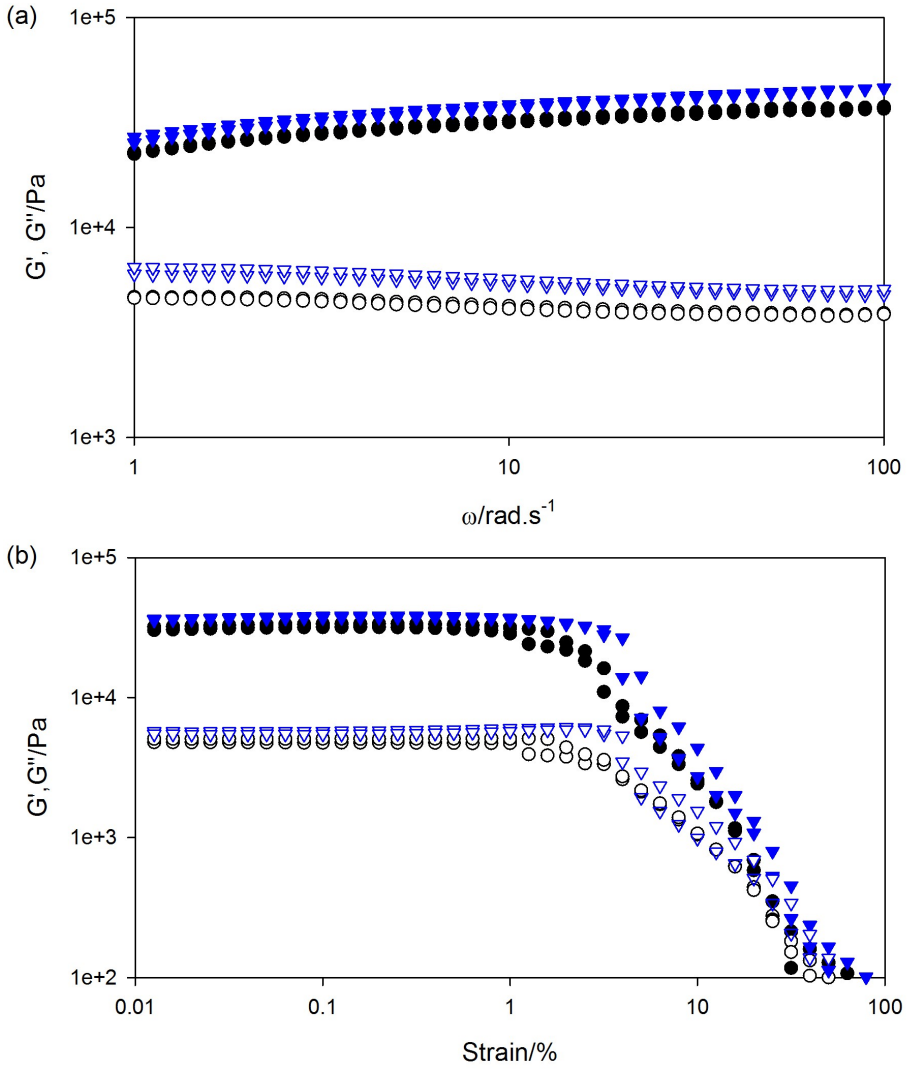

Figure S1i. Plots of G' (solid symbols) and G'' (open) for **2**/$CaCl_2$ gels prepared in (circle) and away from (triangle) the 9.4 T magnetic field of the spectrometer. (a) Frequency sweep measured at 0.5% strain. (b) Strain sweep measured at an angular frequency of 10 rad/s.

The mechanical properties of **2**/$CaCl_2$ gels are not significantly affected by the presence of the magnetic field during gelation. As in our previous work on **1**/GdL gels,[1] the samples prepared in the presence of the magnetic field appear very slightly weaker than the samples prepared away from the field. Samples for these measurements were prepared in D_2O/NaOD at 5 mg/mL **2**, pD 12, without any of the probe molecules listed in Table 1. We previously demonstrated that gels thus prepared possess a degree of alignment with respect to the magnetic field and exhibit similar RQCs to those reported in the current work.[14] Gels were formed in 4 mL Sterilin polystyrene vials which had been roughened with sandpaper to reduce slippage during the measurement. After addition of 140 μL 0.7 M $CaCl_2$ solution, the vials were lowered into the 9.4 T magnetic field of the spectrometer in a homemade cradle and allowed to stand for 48 hours before removal. The gels were analysed, 3 days later, on an Anton Paar Physica MCR 301 rheometer equipped with a vane and cup geometry.

The vial acted as a holder for the gel during the measurement. The samples were prepared at ambient temperature (19-23°C) and maintained at 25°C during analysis.

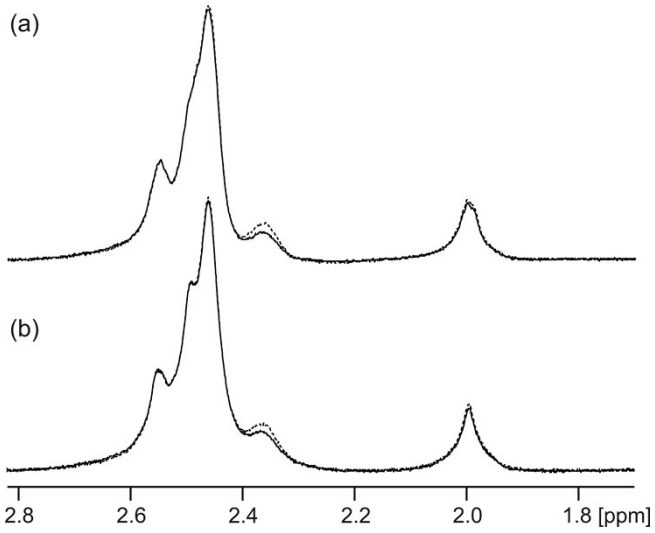

Figure S1j. ^{1}H spectra of probe molecules in **3**/DMSO gel transferred to the NMR spectrometer immediately (< 2 minutes) after preparation and held for 16 hours (a) and a gel held away from the magnetic field (b) with (solid) and without (dashed) on resonance presaturation applied to the gel fibres. Spectra were recorded 16 hours after preparation of the gels.

The presence of the magnetic field does not affect the surface chemical properties of **3**/DMSO gels as very similar STDs are observed to the probe molecules (Figure S1j). The ^{23}Na T_1 and T_2 relaxation times in the sample held away from the magnetic field were measured as 32±2 ms and 20±2 ms respectively, in complete agreement with the values measured in the gel held in the magnetic field for 16 hours.

2. Interpretation of RQC, STD and ^{23}Na relaxation data and justification of experimental protocols

We approximate the interaction of a probe molecule/ion with the gel fibres as a rapid two-site exchange between the probes dissolved in the solution phase and the probes bound to the gel fibres. A spectroscopically observed property of a probe molecule, P_{obs}, is thus the time weighted average of the property in the free and bound states:

$$P_{obs} = f_b P_b + (1 - f_b) P_f \qquad \text{(S2.1)}$$

where f_b is the fraction of molecules bound to the fibre at any instant in time and P_b and P_f are the properties in the free and bound states respectively. A decrease in the affinity of a probe molecule for the surface of the fibres manifests as a smaller value of f_b, and thus a measurably different P_{obs}, provided f_b and the difference between P_b and P_f is sufficiently large. Equation S2.1 has been successfully applied to the interpretation of NMR relaxation,[5, 6] chemical shift[7], STD[8, 9] and RQC[10] data in a variety of different systems.

2.1. RQCs and RDCs

We have previously presented an interpretation of RQC measurements in supramolecular hydrogels.[1] Briefly, nuclei possessing spin quantum numbers (N) greater than ½ possess multiple (2N) NMR transitions. In solids, the transitions are typically split by hundreds of kHz – the quadrupolar coupling – and the lineshapes of quadrupolar nuclei are dominated by the quadrupolar interaction.[11] In isotropic solutions, however, the quadrupolar interactions are averaged to zero by rapid molecular tumbling. The resonances of deuterated organic solvents and symmetrically hydrated ions such as $^{23}Na^+$ and $^{14}NH_4^+$ are thus sharp in H_2O solution with linewidths of only a few Hz. Following Equation S2.1, the lineshape of a probe molecule in exchange with the gel fibres will be a superposition of the lineshapes in the free (solution) and bound (solid-like) states. We write the quadrupolar coupling of a molecule in the bound state, Δ_b, as:[12]

$$\Delta_b = \frac{3\chi}{4I(2I-1)}\left(3cos^2\theta_b - 1\right) \qquad \text{(S2.2)}$$

where χ is the quadrupolar coupling constant and θ_b is the angle between the external magnetic field and the main component of the electrical field gradient at the observed nucleus of the probe molecule in the bound state. It is reasonable to assume that the probe molecule will visit many different gel fibres and binding orientations on a timescale much shorter than that of the NMR experiment.[13] The effective Δ_b, $\Delta_{b,eff}$, will thus be averaged over the many sites visited:

$$\Delta_{b,eff} = \frac{3\chi}{4I(2I-1)}\left\langle 3cos^2\theta_b - 1\right\rangle \qquad \text{(S2.3)}$$

where the brackets <> denote a time average. Thus, if the gel fibres are isotropically arranged, $\Delta_{b,eff}$ is averaged to zero and no quadrupolar coupling is observed.[14] However, if a slight anisotropy in the orientations of the fibres is introduced by preparing the gels in the magnetic field of the spectrometer then $\Delta_{b,eff}$ is non-zero and an RQC (Δ, Figure 2) may be observed, provided χ is of sufficient magnitude. RQCs are thus very sensitive to the molecular structure of the probe; in IPA, an RQC is observed only for the central (methanetriyl) deuteron and not for the methyl groups. As the quadrupolar coupling in the free (solution) state is zero, the magnitude of an RQC is directly proportional to f_b (Equation S2.1). However, the proportionality constant, $\Delta_{b,eff}$, depends upon the anisotropy of the gel fibres and so could potentially change during the gelation process. Nevertheless, as the probe molecules are together in the same sample, a decrease in the fibre anisotropy would decrease the RQCs of all probes to similar extents. In this work, we thus consider the relative changes in the RQCs of two or more complementary probe molecules during the gelation process.

Residual dipolar couplings (RDCs) arise as a result of the through-space coupling of nuclei. In this work, the RDCs within groups of chemically equivalent protons are considered. Only these protons, such as the methyl protons in methylammonium (Section 9) or the CH_2 protons in maleate (Section 10), possess the necessary proximity for RDCs to be observed. The line splitting depends on the number of protons in a group,[15] such that 1:2:1 triplets are observed for methyl groups while doublets are observed for maleate. The dipolar interaction between two nuclei depends upon the term $\langle 3cos^2\theta - 1\rangle$, where θ is the angle between the internuclear vector and the magnetic field and the brackets denote a time average.[16] RDCs are thus observed when the molecules interact with anisotropically arranged gel fibres and can be considered analogous to RQCs in this work.

2.2. ^{23}Na Relaxation

The theory of ^{23}Na relaxation is discussed extensively elsewhere[17-19] and only a brief outline is presented here and in our previous work.[1] The analysis differs slightly from that of RQCs in that the relaxation rate of $^{23}Na^+$ in the solvent phase must be taken into account. The observed relaxation rate, $1/T_{obs}$, is thus:[20]

$$\frac{1}{T_{obs}} = f_b\frac{1}{T_b} + (1 - f_b)\frac{1}{T_f} \qquad \text{(S2.4)}$$

where T is the relaxation time constant in the free (T_f) or bound (T_b) states. Rearranging this equation:

$$\left(\overline{T_{obs}}^{-} - \overline{T_f}^{-}\right) = f_b\left(\overline{T_b}^{-} - \overline{T_f}^{-}\right) \qquad \text{(S2.5)}$$

The minimum in T_{obs} thus occurs at the maximum in f_b. It is apparent from Figure 3 that the maximum in the $^{14}NH_4^+$ RQC coincides with the minimum in the $^{23}Na^+$ T_2 relaxation time, in good agreement with the theory presented here. We note that ^{23}Na relaxation is inherently biexponential in nature due to the different relaxation rates of the central (m = -1/2↔1/2) and 'satellite' (m = -3/2↔-1/2, 1/2↔3/2) transitions. However, in our systems,[1, 21, 22] the molecular motions are generally sufficiently fast for a monoexponential relaxation to be observed and for an effective monoexponential T_1 and T_2 to be determined.[17] T_2 is more sensitive than T_1 to changes in the mobility of the $^{23}Na^+$ ions.[17, 18] However, a smaller decrease in mobility is required for T_2 to become biexponential in nature which can make its meaningful quantification very difficult. The observation of biexponential T_2 relaxation is good evidence for a strong interaction of $^{23}Na^+$ with the gel fibres (Section 8). In our systems, T_1 is always monoexponential. In this work, we are only interested in relating changes in the observed relaxation times to changes in f_b for $^{23}Na^+$ using Equation S2.5. As such, we either quote the effective monoexponential T_1 and T_2, or for systems in which T_2 is strongly biexponential, T_1 only. In systems where T_2 is biexponential, such as 4 mg/mL solutions **2** at pH 9 (Section 8), T_1 is found to be sufficiently reduced from its value in the absence of gel fibres (T_f) for changes in f_b during gelation to be adequately determined.

2.3. Saturation Transfer Difference (STD) Measurements

A detailed protocol for the analysis of protein-ligand binding by saturation transfer difference measurements has been presented by Angulo *et al.*[9] and applied to study the interaction of guest molecules with self-assembled gels by Segarra-Maset *et al.*[23] In our work, we study the interactions of a set of relatively weakly interacting probe molecules with the gel fibres during the gelation process in order to infer how the surface chemical properties of the gels are changing. Our procedure for the collection and interpretation of STD data thus differs from the procedure described by these authors. We quantify the magnitude of an observed STD effect, STD_{obs}, as the difference in the integral of the probe molecule resonance with (I_{sat}) and without (I_0) on-resonance saturation applied to the gel fibres, normalised by I_0:

$$STD_{obs} = \frac{I_0 - I_{sat}}{I_0} \qquad \text{(S2.6)}$$

Our definition of STD_{obs} thus differs from the 'STD-amplification factor' used in the above works as we do not consider the ratio of probe molecules to binding sites; the concentration of probe molecules is constant throughout the experiment while the nature and number of binding sites on

our gel fibres is unknown and likely to change during the gelation process.[1] STD_{obs} can be considered directly proportional to f_b (Equation S2.1), provided that the total concentration of probe molecules and the number of binding sites is constant.[8, 9] However, were the number and nature of binding sites to change, the proportionality constant between f_b and STD_{obs} may also change as a consequence of partially saturated probe molecules being less able to take up more saturation than non-saturated molecules.[9] In our work, the proportionality constant is ideally constant throughout the gelation process so that changes in the affinity of our probe molecules for the gel fibres can be followed. The solution to this problem, as presented by Angulo *et al*.,[9] is to consider not the absolute size of STD_{obs} but rather the initial growth rate of STD_{obs} as a function of the saturation time, t_{sat}. The build-up of STD_{obs} with t_{sat} can be described by the equation:[9]

$$STD_{obs}(t_{sat}) = STD_{max}\left[1 - exp(-kt_{sat})\right] \qquad \text{(S2.7)}$$

where k is an arbitrary constant and STD_{max} is the maximum STD_{obs} attainable (i.e. at very long t_{sat}). The initial growth rate is thus $kSTD_{max}$. The relatively weakly interacting probe molecules in our work give only small STD effects, with much larger STDs observed to the compounds **D1** and **D4** (Section 5). As such, it is not always possible to obtain good fits of our data to Equation S2.7 as STD_{obs} is often too small to be accurately determined at short t_{sat}. Indeed, with **1**/GdL gels (Figure 3) only IPA, acetone, and tBuOH gave STD_{obs} values large enough for k and STD_{max} to be determined. However, our probe molecules are unlikely to spend sufficient amounts of time bound to the gel fibres for the re-binding of saturated probe molecules to present a significant problem.[9]

Plots of STD_{obs} measured at a t_{sat} of 8 s ($STD_{obs,8s}$), $kSTD_{max}$ and STD_{max} are qualitatively the same for IPA, acetone and tBuOH (Figure S2a below). Data for $kSTD_{max}$ is only plotted where the R^2 value for the fitting of the STD build up curves to Equation S2.7 is greater than 0.9. For all other probe molecules, $STD_{obs,8s}$ was always less than 0.1 with R^2 values less than 0.8 and so the fitted values of k and STD_{max} are unreliable. In this study, STD_{obs} measured at 8 s saturation time is plotted as standard for all probe molecules. Although not strictly quantitative, this measure is adequate to prove the increased interaction of the organic solvents with the gel fibres during the formation of **1**/GdL gels.

STD build-up curves (Figure S2a, d) were obtained by varying the number of Gaussian pulses from 10 to 157 while keeping the total length of the presaturation and relaxation delays constant at 8.1 s. STD build-up curves were acquired with 8 scans (on and off-resonance) but no dummy scans, owing to the limited time available during the gelation experiment. The slight (≤ 3%) apparent STDs observed in the absence of a gel are thus relaxation artefacts owing to the first off-resonance scan being acquired before the first on-resonance. Very similar STDs are observed in a final **1**/GdL sample when 16 dummy scans are run before signal acquisition and when a long relaxation delay is elapsed to allow the sample to relax to thermal equilibrium between scans (Figure S2b). Working with **2**/$CaCl_2$ gels, the methylammonium STDs (Section 9) were identical when on resonance saturation was applied at either -5 or 15 ppm and off-resonance at either -100 or 250 ppm. However, when off-resonance presaturation was applied at -50 ppm the STDs were smaller implying appreciable excitation of the fibres even at this high shift (data not shown).

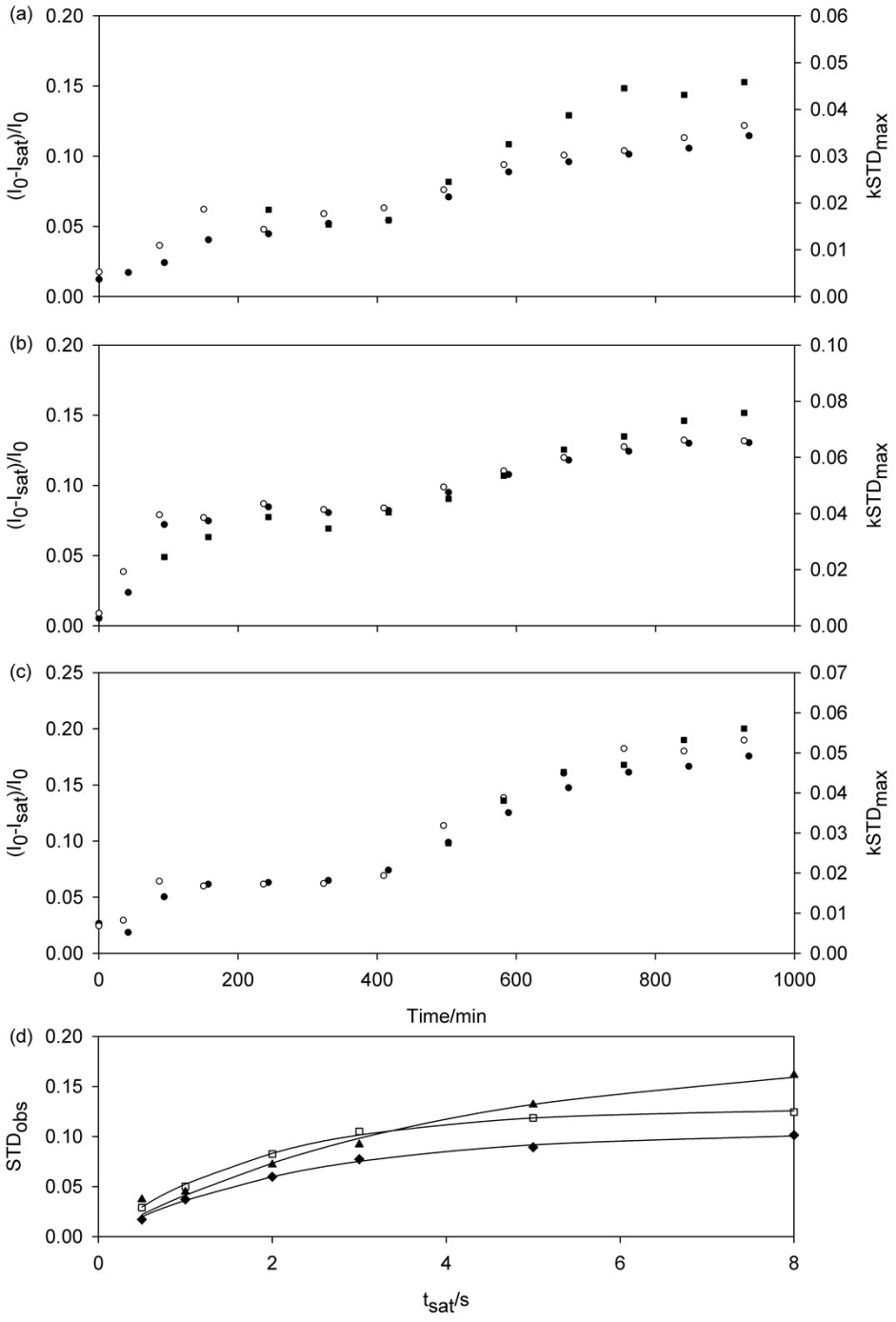

Figure S2a. Plots of $kSTD_{max}$ (square), STD_{max} (white circle) and $STD_{obs,8s}$ (black circle) versus time since addition of GdL to a solution of **1** at pH 9: IPA (a), tBuOH (b) and acetone (c). Sample is the same as Figure 3c, d. (d) Plots of STD_{obs} versus t_{sat}, measured 750 minutes after the addition of GdL: IPA (diamond), tBuOH (white square) and acetone (triangle). Fits to Equation S2.7 are shown as solid lines.

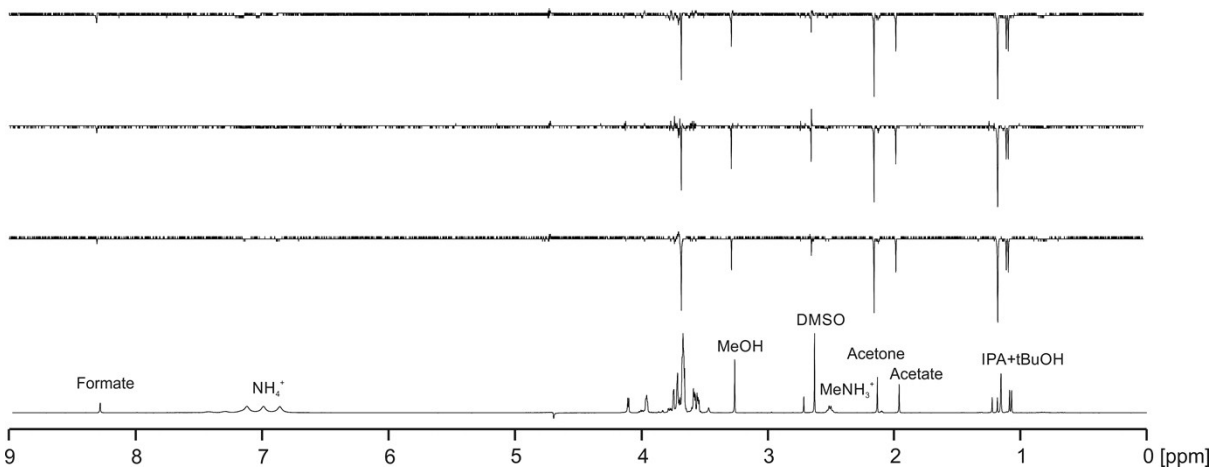

Figure S2b. ^{1}H NMR spectrum of **1**/GdL gel 2700 minutes after the addition of GdL and STD difference spectra (I_{sat}-I_0) recorded with 16 dummy scans, 8 scans and 8.1 s relaxation delay (bottom), no dummy scans (middle) and with a relaxation delay of 40 s (top). The longest T_1 of the probe molecules is 6 s (acetone, formate) so 40 s is adequate to attain thermal equilibrium. The difference spectra have all been scaled by a factor of 10 relative to the reference spectrum.

2.4. Effect of gel syneresis on RQC, STD and ^{23}Na relaxation measurements

With RQC measurements, syneresis gives rise to two separate sets of peaks on the ^{2}H or ^{14}N NMR spectra: a singlet (isotropic) peak for the exuded fluid and a doublet for the gel. ^{2}H and ^{14}N NMR spectra and time-lapse photography of **1**/GdL gels during syneresis are presented in our previous work.[1] The RQC is thus measured only in the gel phase. Owing to the increased density of the gel phase upon syneresis, the RQCs may be expected to increase. However, if syneresis decreases the anisotropy of the fibres with respect to the magnetic field of the spectrometer, the RQCs may instead stay the same or diminish in magnitude. With STD measurements, the probes in the exuded fluid will not exhibit STDs, but will contribute to the calculated STD (Equation S2.6). However, the probe molecules in the gel phase will exhibit enhanced STDs owing to the increased fibre density. Without any decrease in surface area per unit mass of fibre, the observed STDs would remain constant upon syneresis. The increase in the STDs to the organic solvents upon syneresis of **1**/GdL gels (Figure 3d) thus indicates an increased hydrophobicity of the network. The ^{23}Na relaxation should, in principle, exhibit separate components for the exuded fluid and the gel. However, due to the similar relaxation rates in the two phases and the relatively small volume fraction of the exuded fluid[1] (< 30% in **1**/GdL gels), an effective monoexponential relaxation is instead observed.

3. Interaction of dioxane and gluconate with **1**/GdL gels

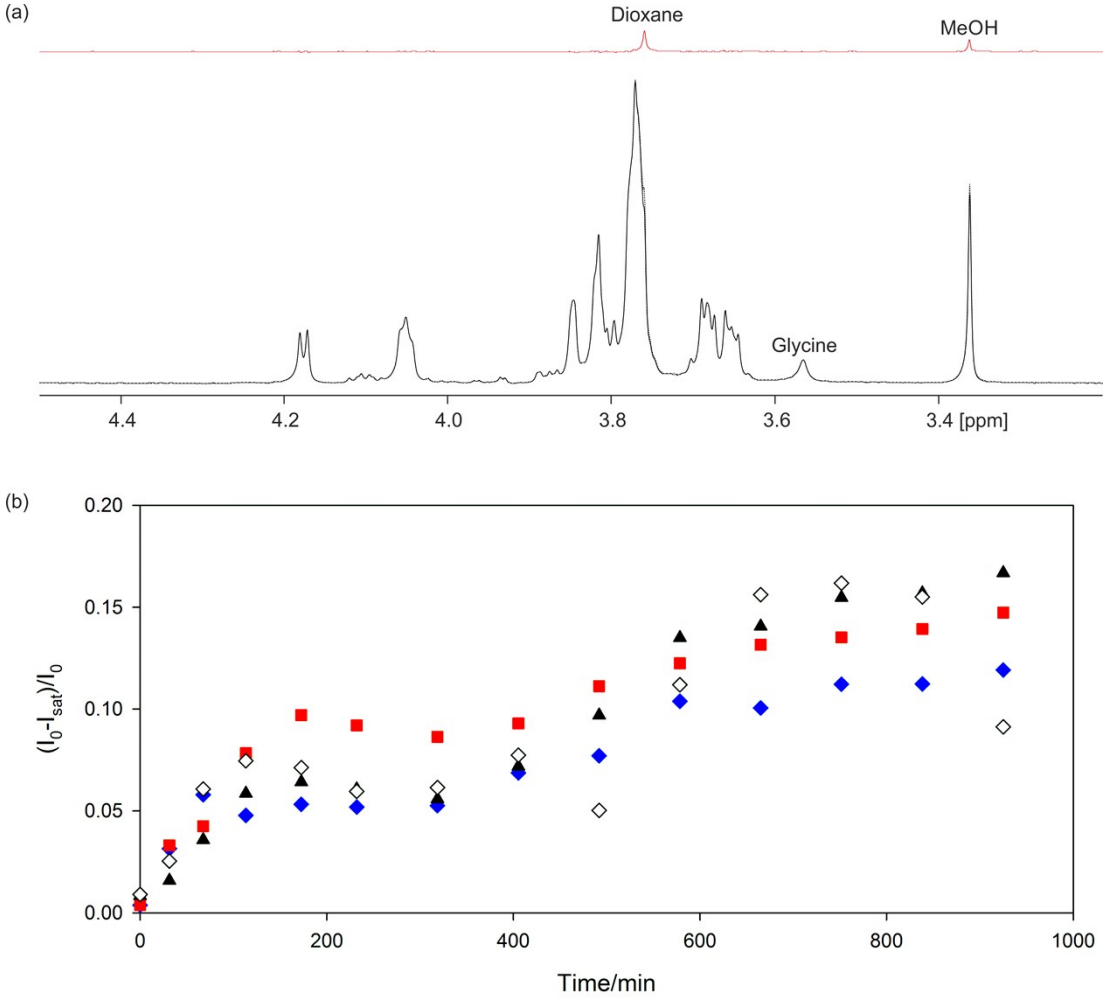

Figure 3. (a) ^{1}H NMR spectra of a **1**/GdL sample, 930 minutes after the addition of GdL, with (solid) and without (dashed) on-resonance presaturation applied to the gel fibres. The difference spectrum (I_0-I_{sat}) is also plotted above (red). All resonances, unless otherwise stated, belong to gluconate with the small peaks assignable as GdL.[24] STDs are only detectable to dioxane and MeOH. (b) Plot of STDs to acetone (black triangle), tBuOH (red square), IPA (blue diamond) and dioxane (white diamond). Dioxane STDs were calculated by normalising the integral of the difference spectra to the spectrum acquired before the addition of GdL. The dioxane STDs are thus affected by any instrumental instabilities over the course of the experiment as well as any slight variability in the GdL and gluconate resonance between the on and off resonance acquisitions. Nevertheless, it can be deduced that the dioxane STDs are similar in size to those of the other organic solvents plotted.

4. Other H^+-triggered hydrogels

4.1. **3**/GdL hydrogels

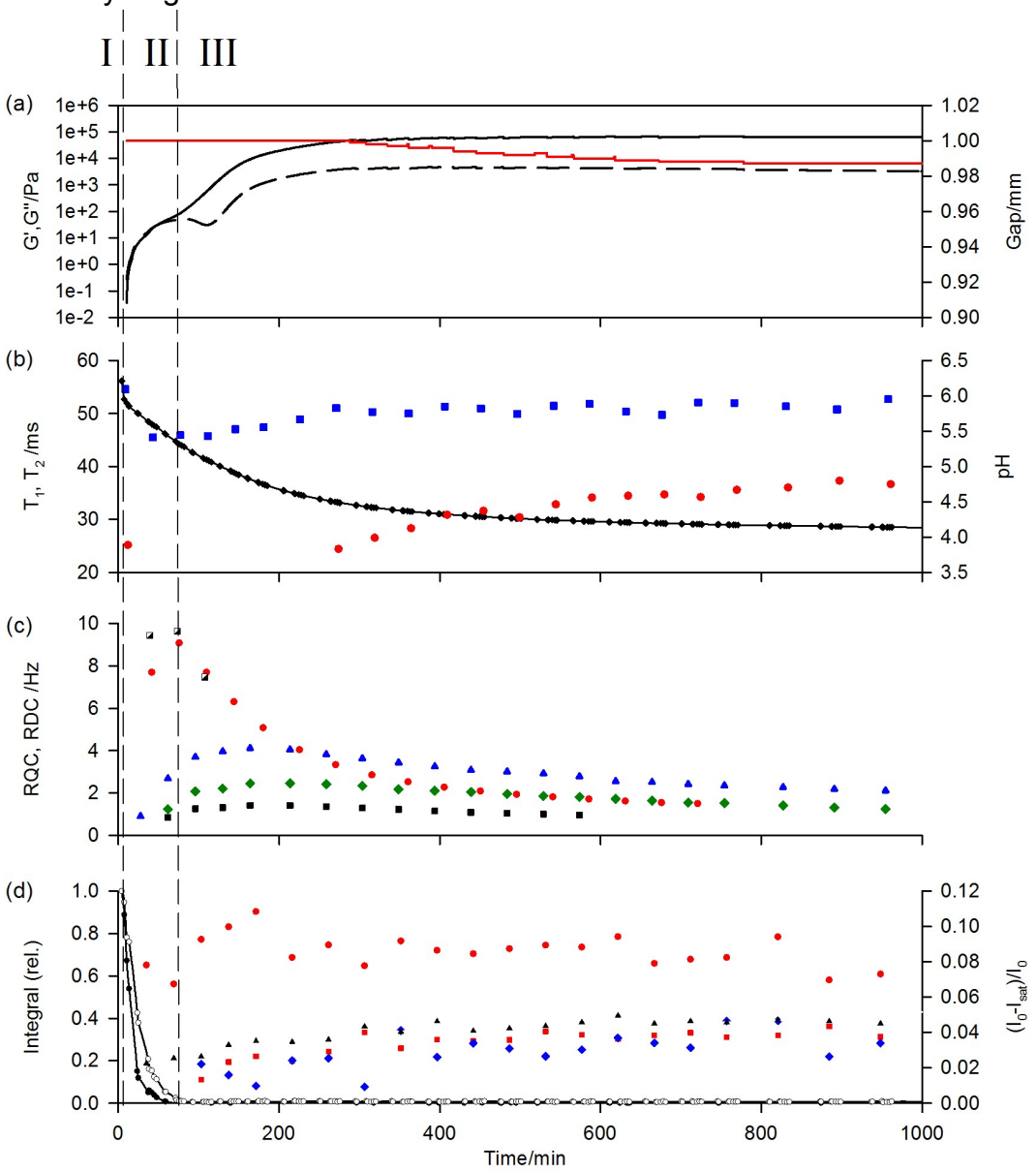

Figure S4a. Plots of experimental observables versus time since the addition of 5 mg/mL GdL to a 5 mg/mL solution of **3** at high pH. (a) Plot of G' (black, solid line) and G'' (dashed) along with the gap between the plates of the rheometer (red). (b) Plot of $^{23}Na^+$ T_1 (blue square) and T_2 (red circle) relaxation times along with pH (black diamond). T_2 is not plotted between 12 and 270 minutes due to the very fast relaxation of the quadrupolar 'satellite' peaks of $^{23}Na^+$; the fitted T_2 values from Equation 2 are misleading. (c) Plot of $^{23}Na^+$ (red circle), IPA (blue triangle), tBuOH (black square) and dioxane (green diamond) RQCs and $MeNH_3^+$ residual dipolar coupling (RDC) (black and white square). The $^{23}Na^+$ RQC has been scaled down by a factor of 20. (d) Plots of ^1H integrals of **3**: leucine CH_3 (white circle) and aromatic protons (black circle). The lines are a guide to the eye. Integrals are normalised to their value at the first spectrum recorded rather than in the absence of GdL. Plot of STDs to probe molecules: IPA (blue diamond), acetone (black triangle), tBuOH (red square) and $MeNH_3^+$ (red circle). No other probe molecules gave significant STDs. $^{14}NH_4^+$ RQCs were too strong to be observed before 300 minutes and are not plotted.

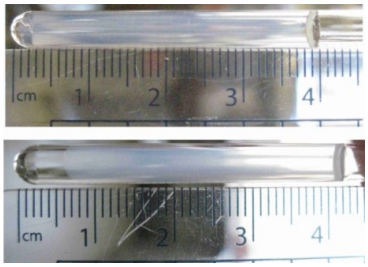

Figure S4b. Comparison of **3**/GdL gel (top) and **1**/GdL gel of Figure 3 (bottom), 40 hours after addition of GdL. A very small amount of syneresis is apparent in the **3**/GdL gel at the base of the NMR tube.

The experimental observables during formation of **3**/GdL gels (Figure S4a) follow a very similar pattern as in **1**/GdL gels: negatively charged structures form during Phase II that lose charge during Phase III while the bulk mechanical properties of the gel increase. The affinity of the organic solvents for the gel increases during both Phase II and Phase III. RQCs (c) are observable for IPA, acetone and dioxane but not tBuOH, while STDs can be observed to all four solvents. Dioxane STDs are not plotted due to overlap with GdL. The binding geometry of the organic solvents around **3**/GdL gels is thus subtly different to that around **1**/GdL gels. The decrease in the magnitudes of the RQCs after 200 minutes indicates a decrease in the anisotropy of the fibres as the STDs remain constant over the same period. Syneresis of the gel also occurs, although to a lesser extent than in **1**/GdL gels (Figure S4b). As in **1**/GdL gels, more polar or negatively charged molecules such as DMSO, MeOH or formate do not show RQCs or STDs.

To prepare **3**/GdL gels, 5 mg/mL of solid **3** was dispersed in a solution containing the set of probe molecules used for **1**/GdL gels. 1.1 equivalents of NaOH were then added and the sample swirled and ground with a PTFE rod for five minutes to dissolve solid **3**. The solution was then filtered using a Pasteur pipette containing a plug of cotton wool in order to remove a small amount of residual solid. The solution was then added to 5 mg/mL GdL and transferred to an NMR tube for analysis. No turbidity was observed in the solution indicating minimal deprotection of the FMOC group. All NMR data on Figure S4a was recorded on the same sample. STDs to the probe molecules were recorded with 5 s presaturation and with on and off-resonance scans recorded in separate 8 scan acquisitions. STDs recorded on a different sample with 8 s presaturation followed identical profiles (data not shown).

The observation of RQCs in **3**/GdL gels but not **3**/DMSO gels is attributable to differences in the assembly mechanisms. Evidence has been presented that gels formed *via* the addition of GdL to solutions of dipeptide gelators at high pH initially form a wormlike micellar intermediate upon assembly of the gelators (Phase II).[25] The structures present in this stage are negatively charged and exhibit relatively little association with one another, the samples possessing only weak mechanical properties. In analogy to the wormlike structures formed by **2** at pH 9, these structures could be expected to align in the magnetic field of the NMR spectrometer giving rise to the RQCs observed.[14] Upon addition of H_2O to a solution of **3** in DMSO, spherical aggregates initially form and the sample resembles a turbid, white suspension. A network of fibres then develops at the expense of the aggregates, with the white solution clearing to form a self-supporting gel.[26, 27] The structures thus formed may be much less able to align in the spectrometer field.[28, 29] Alternatively, the gel may develop too quickly during the two minutes required to place the sample in the NMR spectrometer.

However, it is not feasible to transfer the samples to the NMR spectrometer while they remain turbid.

4.2. **2**/glycolic acid gels

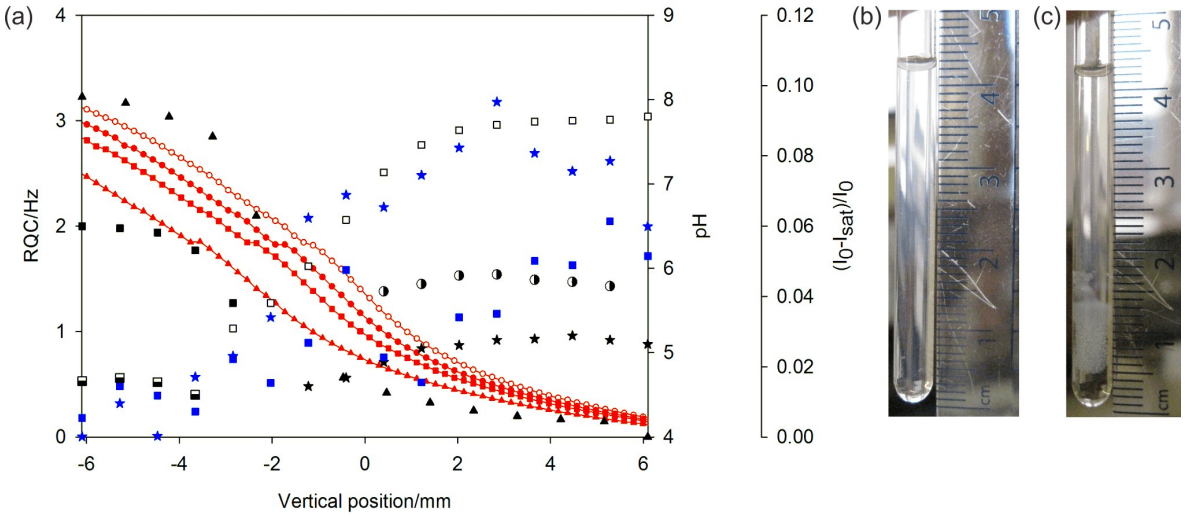

Figure S4c. (a) Plots of observables along length of sample: RQCs (black) of $^{23}Na^+$ (triangle), HDO (square), dioxane (white square), acetone (star), tBuOH (half circle) and MeOH (half black square). $^{23}Na^+$ RQC has been scaled down by factor of 300. No other probes gave observable RQCs. STDs to dioxane (blue square) and acetone (blue star). No other probe molecules gave significant STDs. pH (red) before the $^{23}Na^+$ image (hollow circle), after $^{23}Na^+$ image (solid circle), after ^{2}H dioxane image (square) and after STD image (triangle). The slight inflexion in the pH at 6.5 is an artefact of the pH calculation.[1] 0 mm corresponds to the centre of the NMR active region of the sample. (b) Photograph of gel sample immediately after removal from spectrometer after final pH profile (triangle) was taken. (c) Photograph of gel having stood in water bath at 298 K for seven days.

Gels were formed by placing ca. 1.0-1.2 mg of solid glycolic acid on top of a 4 mg/mL solution of **2** at pH 9 with the full set of probe molecules used for **2**/$CaCl_2$ gels. Glycolic acid was chosen in preference to GdL as its single NMR resonance did not overlap with any of the probe molecules. The gels develop in an analogous way to **1**/GdL and **3**/GdL gels: As the acid diffuses down the tube and the pH falls, charge is removed from the fibres and the $^{23}Na^+$ RQC falls. RQCs and STDs then become apparent to the organic solvents indicating an increase in hydrophobicity. Significant STDs were only observed to acetone and dioxane. No RDCs were observed to maleate or MPA at any stage of gelation. Any RQC of the formate-d ions observed was smaller than the 0.5 Hz observed in **2**/$CaCl_2$ gels, although accurate analysis is impossible owing to the pH dependence of this ion's chemical shift. Having stood in a water bath for seven days, the gel at the bottom of the tube had contracted severely and aggregates had formed (c) while the pH of the sample was 4.3 throughout. STD images were acquired using the same sequence used for ^{1}H images but with the gradient pulse strength, g, varied in 32 steps from -14 to 14 G/cm. Presaturation (5 s) was applied during the relaxation delay (5.1 s) using a train of 98 Gaussian pulses, the pulses as described for one-dimensional STD measurements. 8 scans with on-resonance (-5 ppm) and off-resonance (-250 ppm) presaturation were acquired at each step giving a total acquisition time for both images of 70 minutes.

5. Interaction of model drug compounds with hydrogels

5.1 Interaction of **D1** with **1**/GdL hydrogels

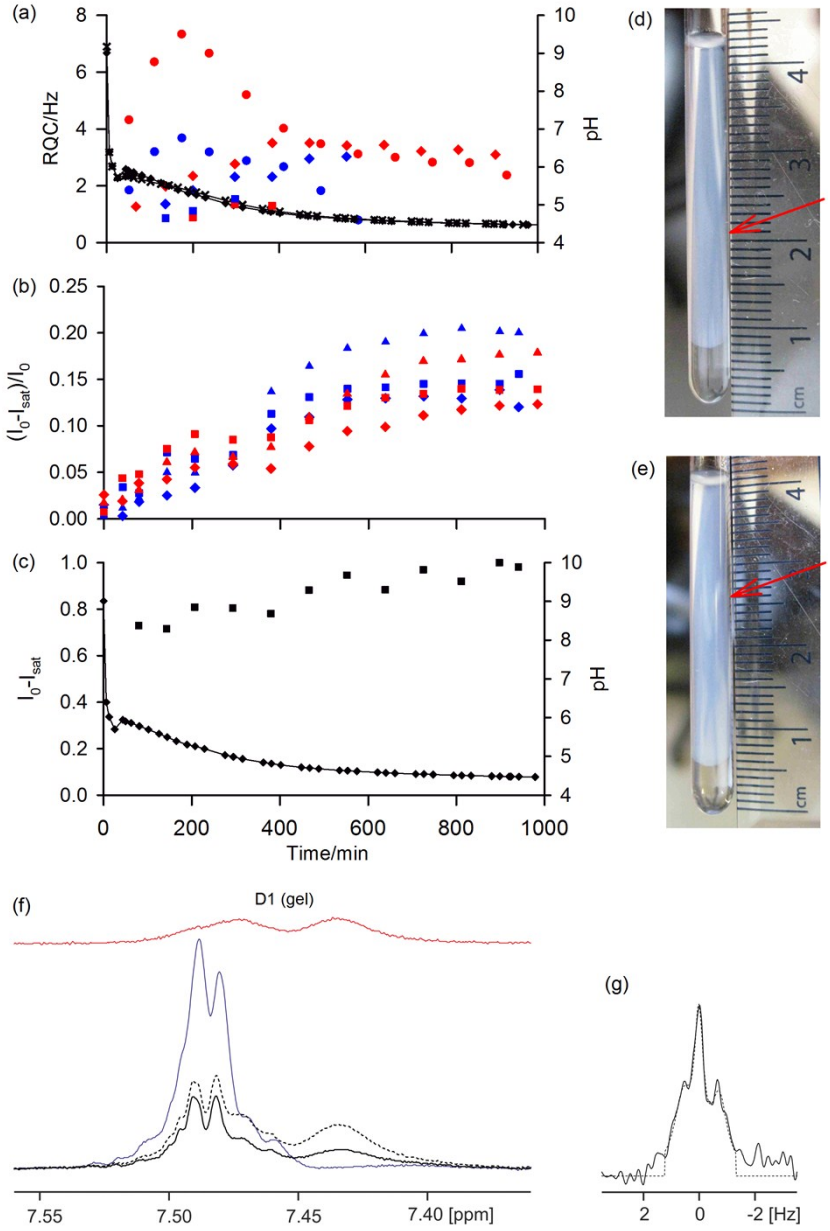

Figure S5a. (a) Plot of RQCs of $^{14}NH_4^+$ (circle), IPA (diamond) and tBuOH (square) with (blue) and without (red) 5 mM **D1** in addition to the standard set of probe molecules used for **1**/GdL gels; both gels contained 10 mM NH_4Cl. Only resolvable RQCs are plotted. The pH is also plotted (black) with (diamond) and without (cross) **D1**. (b) Plot of STDs to acetone (triangle), IPA (diamond) and tBuOH (square) with (blue) and without (red) 5 mM **D1**. (c) Plot of saturation difference of **D1** resonance (square) along with pH (diamond). Photograph of **1**/GdL gel sample containing 5 mM **D1** (d) and without **D1** (e), 17 hours after the addition of GdL. Syneresis (contraction) of the gel is apparent up the edge of the NMR tubes and is indicated with red arrows. (f) ^1H NMR spectra of aromatic resonances of 5 mM **D1** in **1**/GdL gel 940 minutes after the addition of GdL with (solid line) and without (dashed) on-resonance presaturation applied to gel fibres. The difference spectrum is plotted above (red). The spectrum in solution in the absence of **1** is also plotted (blue). (g) ^2H IPA resonance (methanetriyl, 4 ppm) in gel of (f), 900 minutes after the addition of GdL (solid) and approximate Lorentzian deconvolution (dashed).

In the presence of 5 mM **D1**, the $^{14}NH_4^+$ RQC is reduced by approximately 50% (Figure S6a) indicating a preferential binding of **D1** to the fibres. Accurate quantification is difficult due to slight differences in the extent of syneresis between the two samples (d, e). In the following justification, we demonstrate that the binding affinity of **D1** is at least twice that of NH_4^+: **D1** bears a protonated amine group so is presumably able to bind to the same sites as NH_4^+, such as deprotonated carboxylate groups, aided by hydrophobic interactions involving its aromatic ring. If these binding sites are saturated then from Equation S2.1, in the absence of binders other than $^{14}NH_4^+$, the observed $^{14}NH_4^+$ RQC, Δ_{obs}, is given by:

$$\Delta_{obs} = c\frac{S_{tot}}{N_{tot}} \qquad \text{(S5.1)}$$

where: S_{tot} and N_{tot} are the total number of binding sites and NH_4^+ ions respectively and c is a proportionality constant. In the absence of **D1**, doubling the concentration of NH_4^+ from 10 to 20 mM would be expected to decrease Δ_{obs} by 50%. 5 mM **D1** thus has the same effect on Δ_{obs} as 10 mM NH_4^+ and so the binding constant of **D1** to the gel fibres is at least twice that of NH_4^+. We define the binding constant as:

$$K = \frac{[PS]}{[P][S]} \qquad \text{(S5.2)}$$

where PS, P and S denote bound probe, free probe and free binding site respectively. The relatively sharp ^{14}N resonances[1] indicate that the binding sites are unlikely to be saturated with NH_4^+ and so the binding constant of **D1** is likely more than twice that of NH_4^+.

The RQCs (a) and STDs (b) to the organic solvents appear slightly raised in the presence of 5 mM **D1**, possibly due to a cooperative binding effect where **D1** enhances the effective hydrophobicity of the fibres. Accurate calculation of $(I_0\text{-}I_{sat})/I_0$ for **D1** is impossible due to spectral overlap of the aromatic resonances with the NH resonances of **D1**, NH_4^+ and $MeNH_3^+$. Nevertheless, by subtracting this background signal, $(I_0\text{-}I_{sat})/I_0$ can be calculated as 0.42±0.03 for the sample below pH 5. NH protons do not exhibit STDs due to exchange with the solvent. Following initial fibre formation, apparent as an inflexion in the pH,[1, 3] $(I_0\text{-}I_{sat})$ remains large for the remainder of the experiment suggesting a strong interaction with the gel fibres throughout (c).

The strong interaction of **D1** with the gel fibres is readily apparent by ^1H NMR (f). By plotting the difference (red) between the spectra of **D1** obtained with and without presaturation applied to the gel fibres, it is apparent that the resonance of **D1** in the gel phase is very different to that in an analogous solution in the absence of a gel (blue). The peaks are much broader while the multiplicity is also different.[30, 31]

Syneresis of the gel sample extends up the walls of the NMR tube (d, e) and thus into the NMR-active region, centred 18 mm from the base of the tube and extending 8 mm up and down. Deconvolution of the ^2H IPA resonance (g) indicates that approximately 70% of this volume is occupied by gel, the rest by fluid which gives rise to the central singlet peak on (g). The ^1H resonance of **D1** (f) in the fluid exuded during syneresis (upfield, sharp) is thus significant.

5.2 Interaction of **D2**-**D4** with **1**/GdL gels

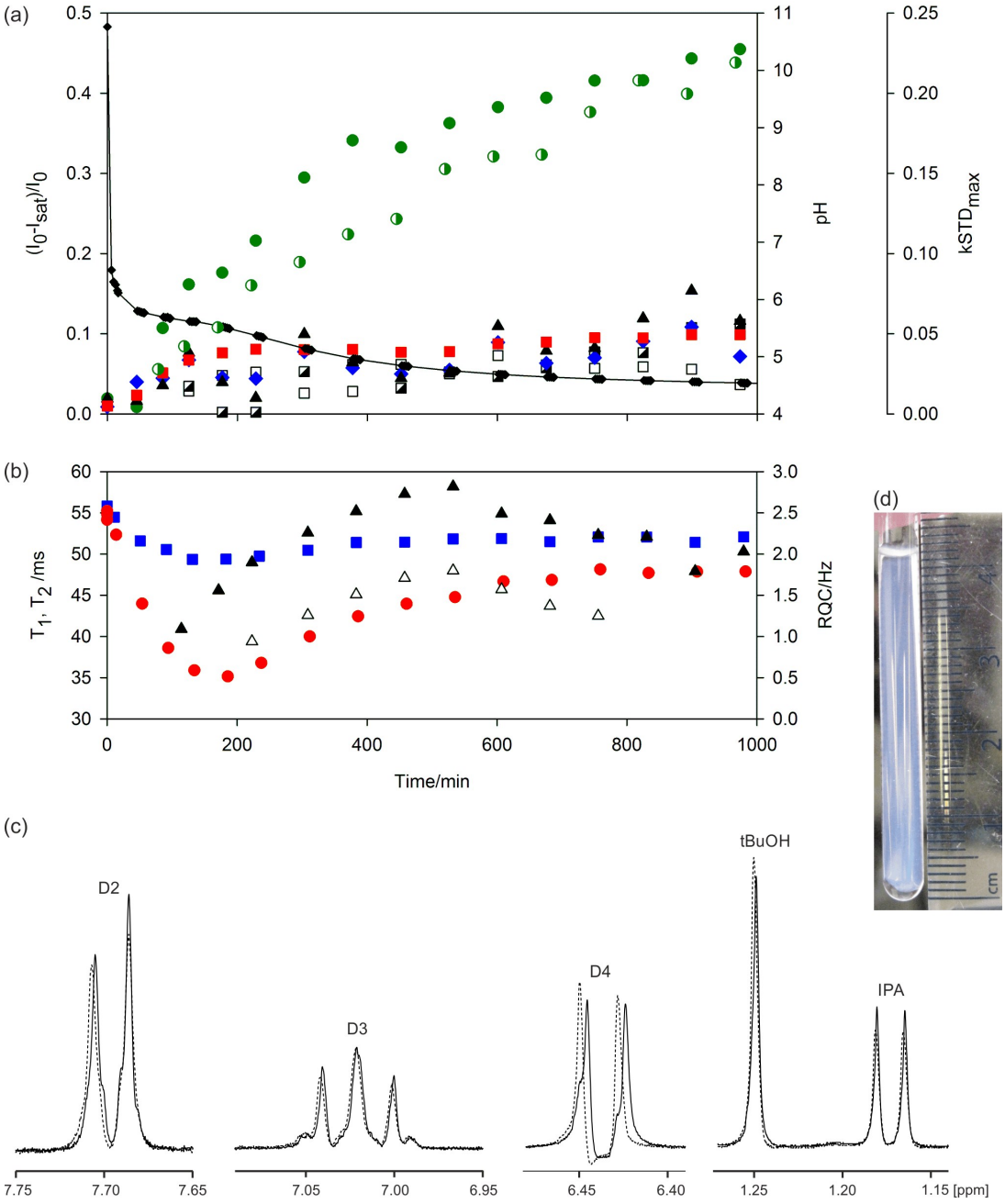

Figure S5b. (a) Plots of STDs to IPA (blue diamond), acetone (black triangle), tBuOH (red square), **D2** (black/white square), **D3** (white square) and **D4** green circle. kSTD$_{max}$ for **D4** (half green circle). (b) Plots of $^{23}Na^+$ T_1 (blue square) and T_2 (red circle) relaxation times along with RQCs of IPA (black triangle) and tBuOH (white triangle). (c) ^{1}H NMR spectra of molecules in **1**/GdL gel at pH 4.4 (solid line), 1700 minutes after the addition of GdL, and in analogous solution in absence of **1** (dashed). Spectra were referenced to sodium methanesulfonate (2.815 ppm). For **D4**, separate resonances are discernible in the **1**/GdL gel for the molecules in the gel (upfield) and in the fluid exuded during syneresis (downfield). Spectra were acquired using a double-echo WATERGATE sequence in 8 scans with a signal acquisition time of 3.7 s and a relaxation delay of 1 s. No line broadening factor has been applied to the spectra. The negative intensity in the centre of the doublet is due to J-modulation. (d) Photograph of gel sample, 1700 minutes after the addition of GdL.

5.3 Interaction of **D1**-**D4** with **2**/$CaCl_2$ gels

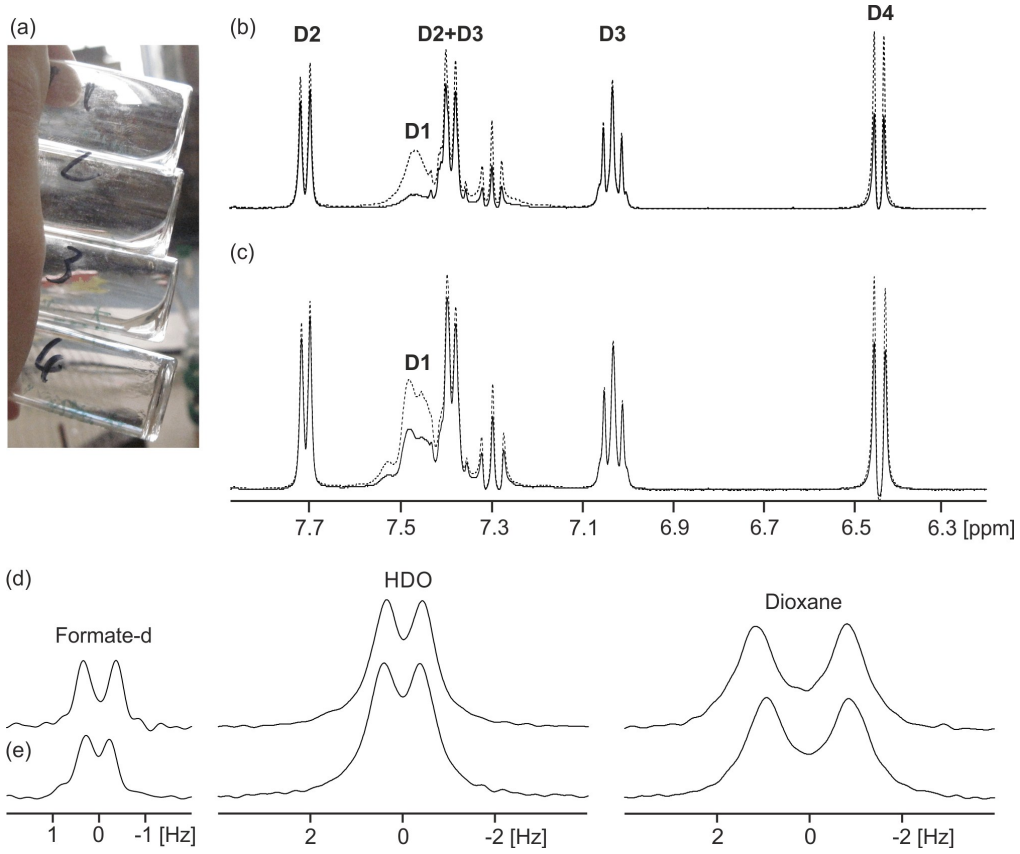

Figure S5c. (a) Photographs of 4 mg/mL solutions of **2** at pH 9 with various model drug compounds, each at 5 mM concentration unless otherwise stated, along with standard set of probe molecules for **2**/$CaCl_2$ gels: **D3** and **D4** (1), 1 mM EDTA (2), **D2**, **D3** and **D4** (3) and **D1**-**D4** (4). (b) NMR spectra of solution of Sample 4, two weeks after the addition of 30 mM $CaCl_2$ (Figure 4d, reproduced here for convenience). (c) NMR spectra of a **2**/$CaCl_2$ gel, prepared using the standard set of probe molecules, with 5 mM **D1**-**D4** diffused into the sample. ^{2}H NMR spectra of probe molecules in the **2**/$CaCl_2$ gel before (d) and after (e) **D1**-**D4** were diffused in.

4 mg/mL solutions of **2** at pH 9 prepared with **D2-D4** are free-flowing while solutions prepared with **D1** are not (a). RQCs were not observed for the solution containing **D1** while the other solutions all exhibited RQCs. These observations indicate a strong interaction between **D1** and the structures of **2** that prevents re-orientation in the presence of the magnetic field. Similar STD effects to **D1**-**D4** are observed when they are included in the solution of **2** prior to the addition of $CaCl_2$ (b, Figure 4d) and when they are diffused into a **2**/$CaCl_2$ gel (c). In both cases, **D1** exhibits the broadest peaks and the strongest STDs. To prepare the sample of (c-e), a **2**/$CaCl_2$ gel was prepared following the standard procedure listed in the main text. A solution was prepared at pH 9 containing 10 mM **D1**-**D4**, pH indicators (2 mM with respect to sodium acetate), 1 mM disodium maleate, ^{2}H organic solvents at 0.05 vol% (0.02 vol% MeOH-d_3) and 0.01 vol% of all ^{1}H solvents (no IPA). Two weeks after the addition of $CaCl_2$ to a solution of **2** to form a gel, ca. 600-640 μL of the **D1**-**D4** solution was placed on top of the gel. The sample was then held in a water bath at 298 K for one month prior to (c, e) being recorded. The RQCs of the probe molecules in the gel show only slight changes as **D1**-**D4** and Na^+ diffuse into the gel and Ca^{2+} diffuses out (d, e).

6. **2**/$CaCl_2$ hydrogel at different stages of gelation

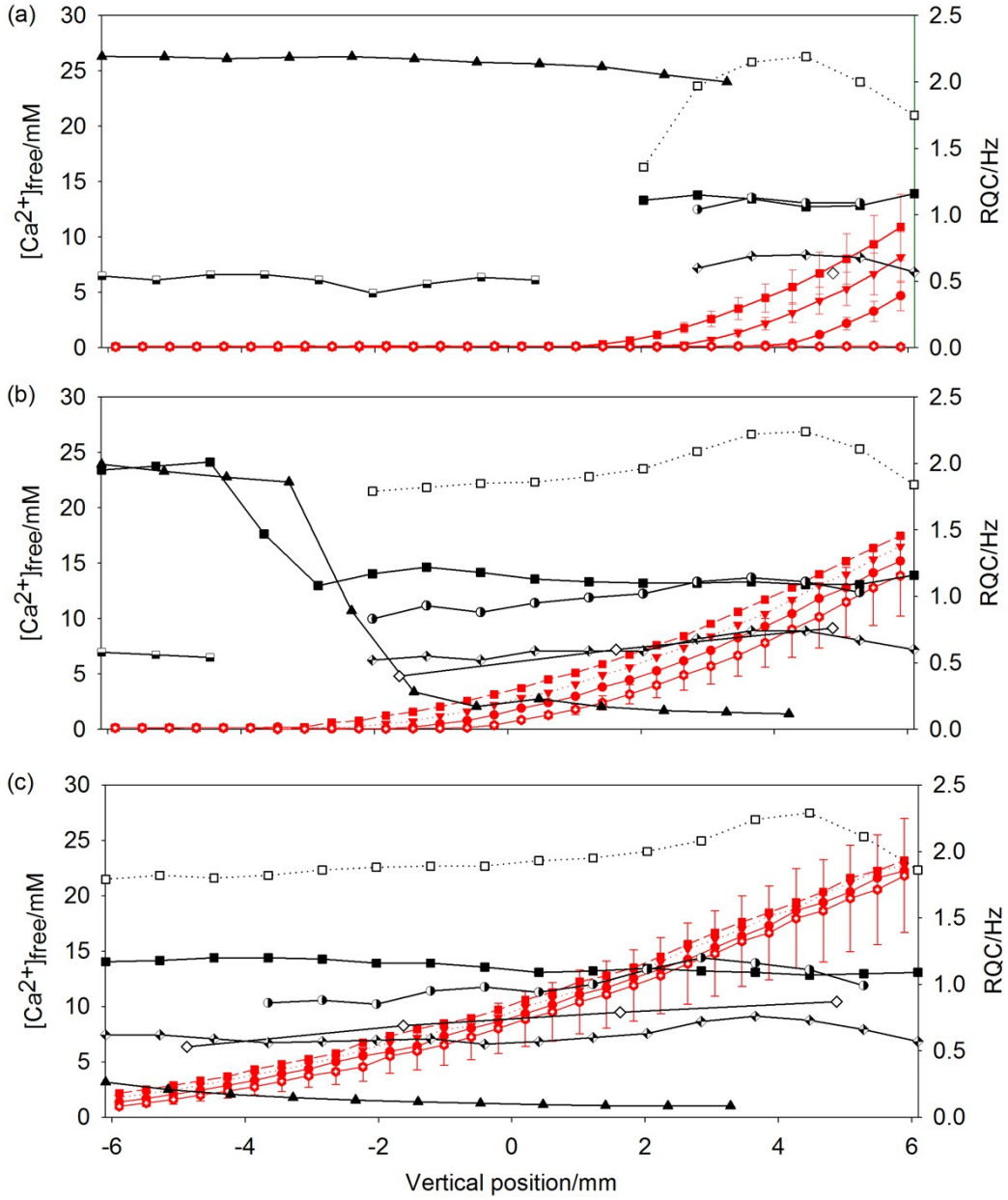

Figure S6. Plots of experimental observables at different stages of a CSI experiment after placing 0.7 M $CaCl_2$ solution on top of a 4 mg/mL solution of **2**: (a) 1 hour, (b) 6 hours and (c) 14 hours. Profiles of RQCs (black): $^{23}Na^+$ (black triangle), formate-d (white diamond), HDO (black square), dioxane (white square), tBuOH (half black circle), acetone (black and white diamond) and MeOH (half black square). The $^{23}Na^+$ RQC has been scaled down by a factor of 500. Red: Profiles of $[Ca^{2+}]_{free}$ before all images (hollow hexagon) – error bars indicate uncertainty in $[Ca^{2+}]_{free}$ measurements – after ^{23}Na image (circle), after formate-d image (down triangle) and after ^2H HDO and dioxane image (square). The lines are to guide the eye.

The 0.7 M $CaCl_2$ solution has a higher density than a 4 mg/mL solution of **2** at pH 9. In the early stages of the experiment, the movement of the Ca^{2+} down the tube can thus be driven by gravity rather than diffusion alone. The apparently anomalous rise in the ^2H dioxane coupling at 4 mm height is likely an artefact of this process. Below this point, the progress of the $CaCl_2$ down the tube was very slow so was likely driven by diffusion alone.

7. *In-situ* $[Ca^{2+}]_{free}$ measurements

As with *in-situ* pH measurements,[1, 7] the observed chemical shift, δ_{obs}, of our Ca^{2+} indicator molecules is a weighted average of the shifts in the bound and free states:

$$\delta_{obs} = f_{Ca}\delta_{Ca} + (1 - f_{Ca})\delta_f \quad \text{(S7.1)}$$

where δ_f and δ_{Ca} are the limiting shifts of the indicator when completely free and bound to Ca^{2+} respectively. fc_a is the fraction of indicators bound to Ca^{2+} at any instant. We define the Ca^{2+} binding constant, K_{Ca}, of maleate(2-) as:

$$K_{Ca} = \frac{[MalCa]}{[Mal][Ca^{2+}]_{free}} \quad \text{(S7.2)}$$

where Mal and MalCa represent free and complexed maleate respectively and the square brackets denote concentration. Combining Equations S7.1 and S7.2:

$$[Ca^{2+}]_{free} = \left(\frac{1}{K_{Ca}}\right)\frac{\delta_f - \delta_{obs}}{\delta_{obs} - \delta_{Ca}} \quad \text{(S7.3)}$$

To obtain K_{Ca}, δ_f and δ_{Ca}, solutions were prepared containing different concentrations of $CaCl_2$ and the following components: 0.1 mM each of disodium maleate, sodium glycolate, sodium methanesulfonate and sodium formate. 0.001 vol% dioxane, methanol, acetone, DMSO and tert-butanol were also included. The water to prepare these solutions (Resistivity 18.2 MΩ.cm) was degassed by bubbling with N_2 for ten minutes. The pH was adjusted from 7 to between 9.7 and 10.5 by the inclusion of 0.2±0.1 mM NaOH. Such a high pH ensures that the maleate is completely in its dianionic form. The total free calcium concentration in solution will not be significantly affected by such a low concentration of base.[32] Likewise, any slight carbonate contamination will not have a significant effect due to the relatively low binding affinity of HCO_3^- for Ca^{2+}.[33] With such a low concentration of weak Ca^{2+} binders, $[Ca^{2+}]_{free}$ can be assumed equal to the total concentration of $CaCl_2$ added.

Maleate was found to be the most sensitive indicator over the $[Ca^{2+}]$ ranges of interest. Plots of δ_{obs} of maleate versus $[CaCl_2]$ in the presence and absence of 50 mM NaCl are shown in Figure S7 below. Good fits to Equation S7.3 were obtained with both data sets, fitting up to 50 mM $CaCl_2$. It is clear, however, that there is competition between Ca^{2+} and Na^+ for maleate as the apparent K_{Ca} is substantially reduced in the presence of 50 mM NaCl (Table S7). The dependence of the apparent K_{Ca} of organic ligands on the concentration of competing alkali metal ions has been well documented.[34, 35] In our work on **2**/$CaCl_2$ gels, we need to measure $[Ca^{2+}]_{free}$ along a $CaCl_2$ gradient in the presence of **2**. We cannot accurately know the solution composition (sodium activity, ionic strength) and thus the apparent K_{Ca} at any particular point along our sample. However, K_{Ca} under our experimental conditions is unlikely to fall outside of the range of values determined in our calibration experiment in the presence/absence of 50 mM NaCl. We thus report $[Ca^{2+}]_{free}$ as the median of the values calculated using the fitted K_{Ca}, δ_f and δ_{Ca} in the presence and absence of 50 mM NaCl, with the difference between the two values as the uncertainty in $[Ca^{2+}]_{free}$. The ^1H resonance of MeOH was used as a chemical shift reference rather than methanesulfonate owing to the very slight sensitivity of the latter to Ca^{2+} (data not shown).

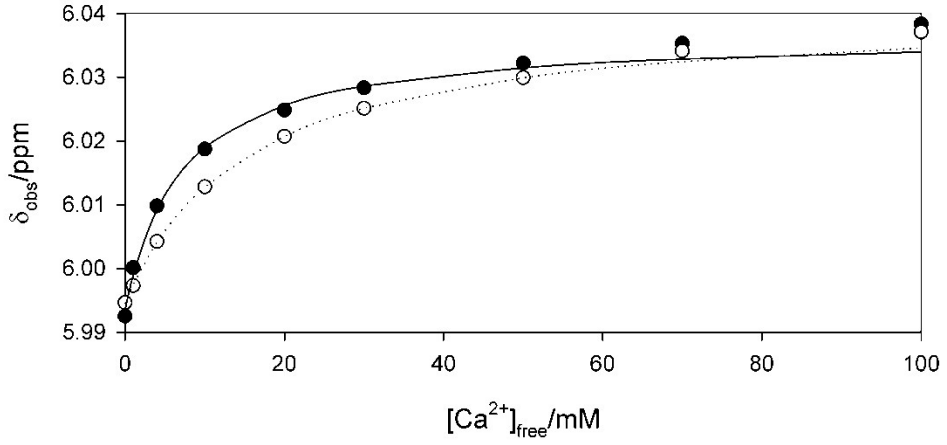

Figure S7. Plot of maleate chemical shift, δ_{obs}, versus $[Ca^{2+}]_{free}$ in the presence (white circle) and absence (black) of 50 mM NaCl. The plotted lines are fits of Equation S7.3 to the data up to 50 mM Ca^{2+}.

[NaCl]/mM	K_{Ca}/M^{-1}	δ_{Ca}/ppm	δ_f/ppm
0	143.37	6.0367	5.9935
50	65.332	6.0407	5.9946

Table S7. Fitted values of K_{Ca}, δ_f and δ_{Ca} with MeOH (3.36 ppm) as a reference.

The chemical shift difference between maleate(2-) and monohydrogenmaleate(-) was estimated as 0.4 ppm (data not shown). Given a pKa of 6.0 for maleic acid,[34] the chemical shift will deviate by less than 0.0013 ppm when the pH is 8.5 or above which is the case in all **2**/$CaCl_2$ samples discussed in this work. Such a shift corresponds to an uncertainty in $[Ca^{2+}]_{free}$ of less than 1 mM.

8. Relaxation of $^{23}Na^{+}$ in 4 mg/mL solutions of **2** and in **2**/$CaCl_2$ gels

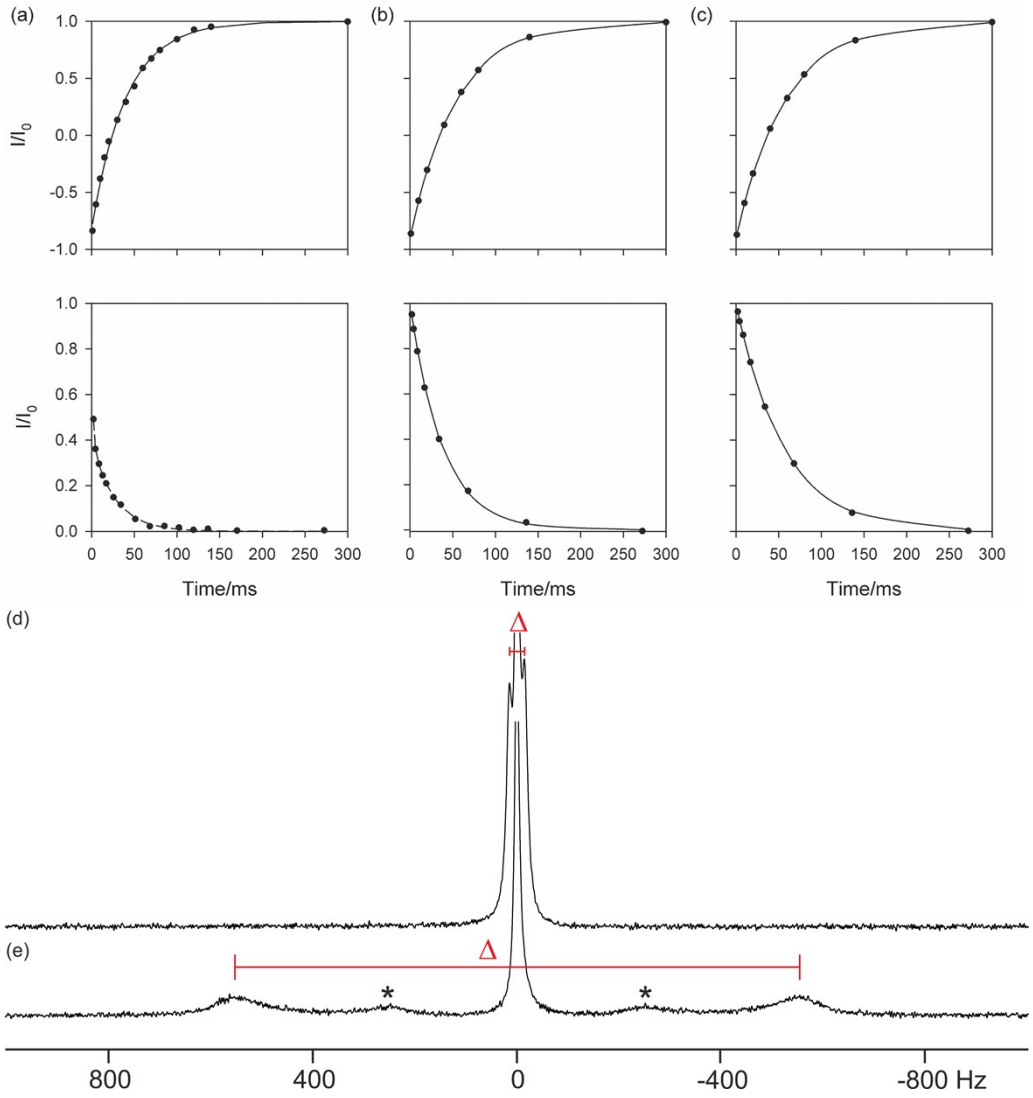

Figure S8a. ^{23}Na T_1 inversion-recovery (upper plots) and T_2 CPMG (lower plots) relaxation curves: (a) 4mg/mL solution of **2** at pH 9 with full set of probe molecules for **2**/$CaCl_2$ gels, (b) **2**/$CaCl_2$ gel seven weeks after addition of $CaCl_2$ and (c) analogous solution in the absence of **2**. Solid lines are fits to Equations 1 and 2. A bi-exponential fit (dashed) was required for T_2 in (a), fitting to Equation 1 of Shinar *et al.*[36] ^{23}Na NMR spectra of **2**/$CaCl_2$ gel seven weeks after addition of $CaCl_2$, $[Ca^{2+}]_{free}$ = 25±6 mM (d) and the same sample before the addition of $CaCl_2$ (e). The RQC (Δ) is indicated. The peaks marked * belong to a minor liquid-crystalline phase of **2**.

In the absence of $CaCl_2$ (a), the T_2 relaxation of $^{23}Na^{+}$ is biexponential with a T_2 of 26 ms for the slow component (central peak) and less than 5 ms for the fast component. The fast component decays completely before the second data point and is unfortunately beyond the resolution of our instrument. T_1 in this sample was measured as 41±1 ms. In the **2**/$CaCl_2$ gel (b), T_2 relaxation is monoexponential with a fitted T_2 of 38±1 ms while T_1 was measured as 54±1 ms. In the absence of **2** (c), T_1 and T_2 are 57±1 and 56±1 ms respectively. These results confirm an increase in mobility of the $^{23}Na^{+}$ upon addition of $CaCl_2$. The reduced magnitude of T_2 so that $T_1 \neq T_2$ confirms a reduced mobility (increased correlation time) of the $^{23}Na^{+}$ ions relative to a dilute aqueous solution. We can thus be confident that the $^{23}Na^{+}$ ions maintain a significant interaction with the gel fibres, even in the

presence of an excess of Ca^{2+}. This is further confirmed by a non-zero RQC of 30 Hz in the final gel (d). ^{23}Na NMR spectra were acquired using a $\pi/2$ pulse (32 μs), a 10 kHz sweep width with 3022 data points. 256 scans were acquired. Relaxation measurements performed along the length of the Ca^{2+} gradient (Figure S8b) show how the T_2 relaxation changes from biexponential and fast in the absence of Ca^{2+} to monoexponential and slow in the presence of excess Ca^{2+}. Spatially resolved ^{23}Na relaxation curves were recorded using a modified version of gradient phase encoding sequence used for ^{23}Na RQC measurements. The pulse sequence was modified to include an inversion-recovery sequence (T_1 image) or a CPMG pulse train (T_2). 8 gradient steps were acquired with 128 scans at 8 delay times at each gradient step (T_1) or 8 different numbers of π pulses (T_2). The acquisition time for the images was 56 minutes for both T_1 and T_2 images. The theoretical spatial resolution is 3.8 mm.

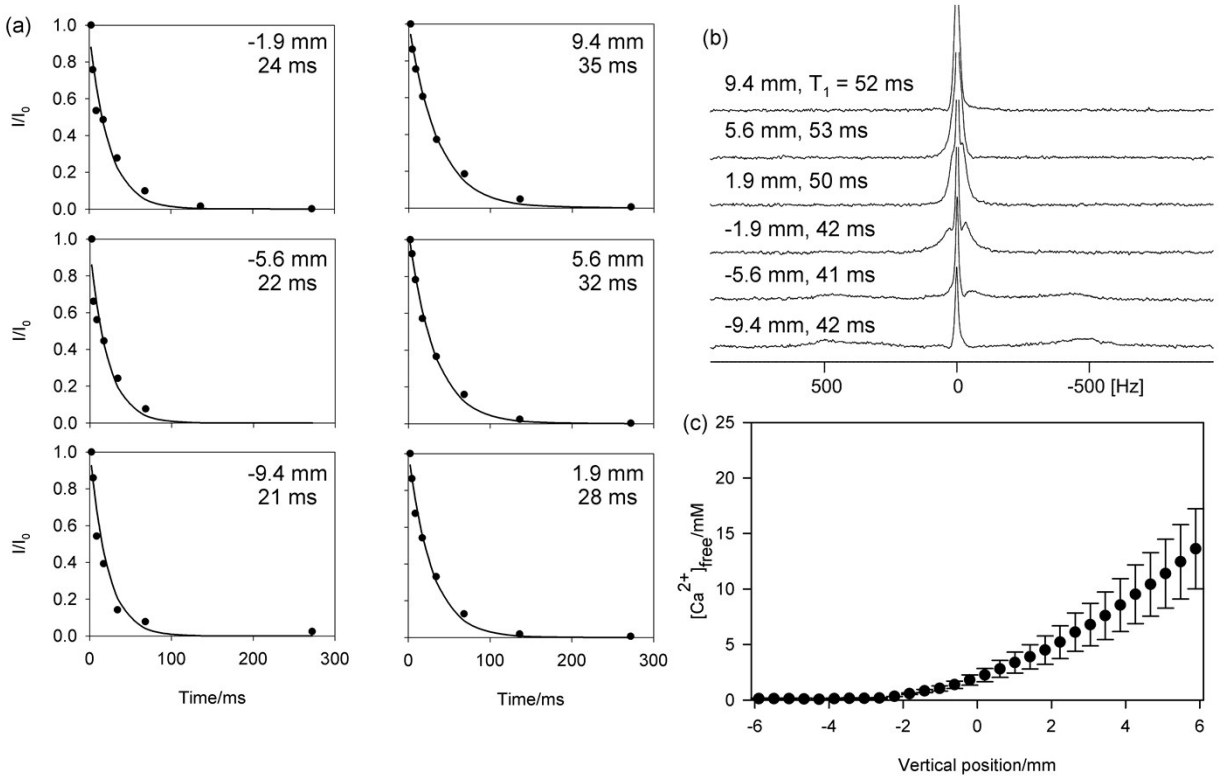

Figure S8b. (a) ^{23}Na CPMG curves recorded at different positions along a Ca^{2+} gradient during formation of a **2**/$CaCl_2$ gel. The monoexponential fits to Equation 2 are shown as solid lines. The vertical position and fitted T_2 values are also given. (b) ^{23}Na NMR spectra from the corresponding positions along with T_1 relaxation times. (c) Plot of $[Ca^{2+}]_{free}$ versus vertical position along the sample. In all cases, T_1 relaxation curves fitted perfectly to a monoexponential fit.

9. Methylammonium as a probe of negative charge in **2**/$CaCl_2$ gels

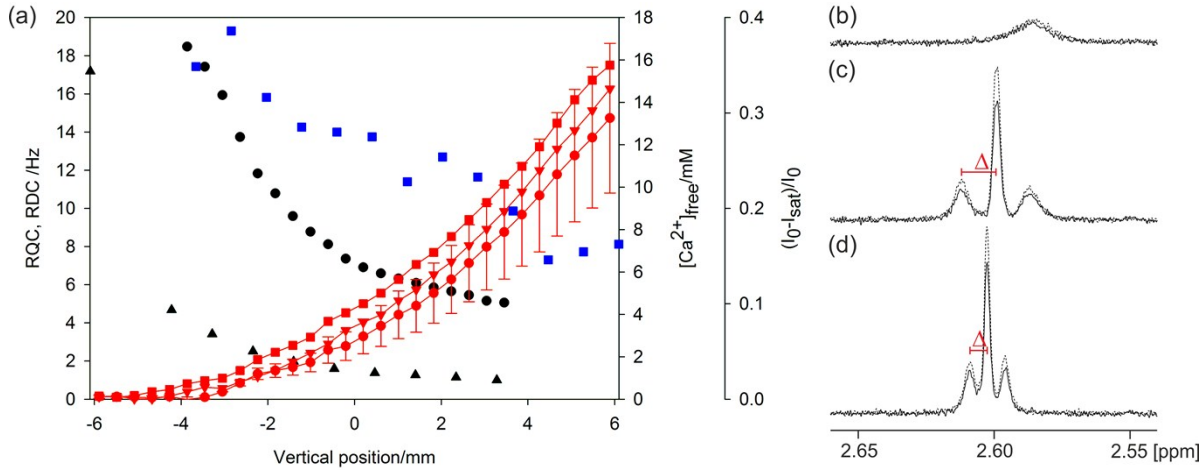

Figure S9. (a) Plots of experimental observables along length of sample: $^{23}Na^+$ RQC scaled down by factor of 50 (black triangle), residual dipolar coupling (RDC) of methylammonium (black circle) and STD of methylammonium (blue square). Plots of $[Ca^{2+}]_{free}$ before all CSI experiments (red circle, with uncertainties shown as error bars), after the ^{23}Na image (red triangle, methylammonium RDCs were acquired from the same ^1H image) and after the methylammonium STD experiment (red square). (b-d): ^1H NMR spectra of the methylammonium resonance with (solid) and without (dashed) on-resonance presaturation applied to the gel fibres. (b) 4 mg/mL solution of **2** in absence of $CaCl_2$. (c) **2**/$CaCl_2$ gel during formation, extracted from STD image (a) at 2.8 mm, at $[Ca^{2+}]_{free}$ of 9±3 mM. (d) **2**/$CaCl_2$ gel three weeks after addition of $CaCl_2$ at $[Ca^{2+}]_{free}$ of 22±5 mM. The RDCs (Δ) are indicated.

In the absence of $CaCl_2$, methylammonium binds strongly to the structures of **2** and gives a very broad resonance. Integration suggests only 30-40% of the methylammonium is NMR-visible. Upon addition of $CaCl_2$, a sharper resonance becomes apparent (c) which is split 1:2:1 by a residual dipolar coupling (RDC). Integration of this resonance shows that all the methylammonium is NMR visible. As more $CaCl_2$ diffuses down the tube, the methylammonium RDC falls in tandem with the $^{23}Na^+$ RQC as well as the methylammonium STD. However, the RDC and STD of methylammonium are appreciable in the final **2**/$CaCl_2$ gel (d) suggesting that methylammonium remains in competition with Ca^{2+}. Methylammonium is thus analogous in its behaviour to $^{23}Na^+$. STD images were acquired as described for **2**/glycolic acid gels in Section 4.

10. Analysis of residual dipolar couplings (RDCs) of different probe molecules in **2**/$CaCl_2$ gels

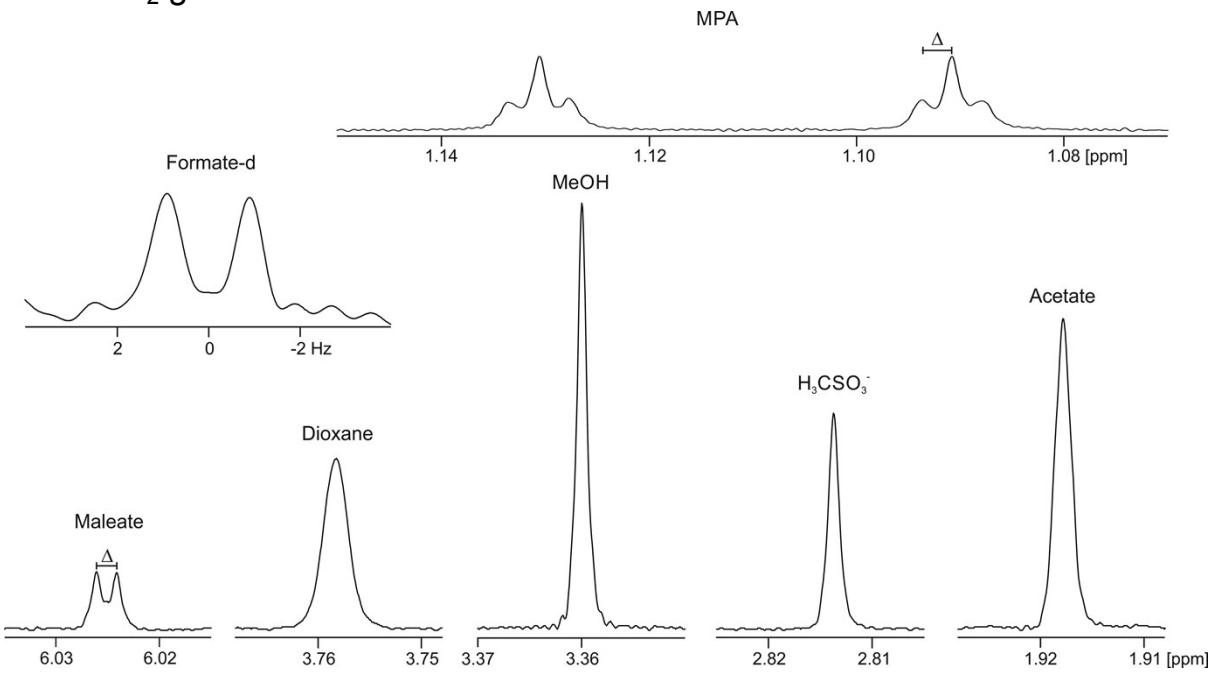

Figure S10. ^{1}H NMR spectra of probe molecules in **2**/$CaCl_2$ gel along with ^{2}H spectrum of formate-d. RDCs (Δ) are observable on the maleate and MPA^{2-} resonances, while weaker Ca^{2+} binders such as acetate and methanesulfonate do not exhibit RDCs. $[Ca^{2+}]_{free}$ in this sample was measured as 24±6 mM throughout. ^{1}H spectra were extracted from a CSI image (off-resonance) recorded as described for **2**/glycolic acid gels (Section 4). ^{2}H spectrum of formate was extracted from the same region of an 8 point CSI image. RQC of formate-d was measured as 0.9 Hz. Sample is shown nine days after the addition of $CaCl_2$. RDCs and RQCs were the same when re-measured six weeks later. Due to the $[Ca^{2+}]_{free}$ dependence of the MPA^{2-} and maleate chemical shifts, RDCs could not be measured during the gel formation process along the Ca^{2+} gradient owing to a slight broadening of the peaks in the CSI image. RDCs were observable on the MPA^{2-} resonance once $[Ca^{2+}]_{free}$ exceeded 10±3 mM and on the maleate resonance after 19±5 mM; in both cases the change in chemical shift with $[Ca^{2+}]_{free}$ was small enough for RDCs to be observed. No RDCs were observed in the absence of Ca^{2+}.

11. ^{43}Ca NMR analysis of a **2**/$CaCl_2$ gel

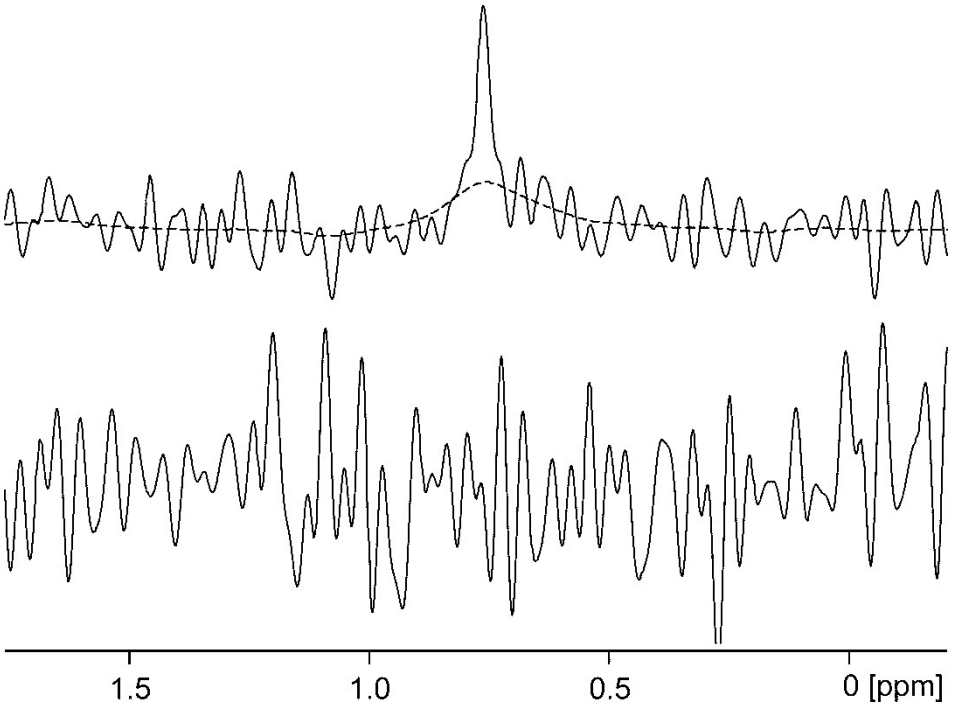

Figure S11. (Top) ^{43}Ca NMR spectrum of a H_2O solution at pH 9 containing 20 mM $CaCl_2$ and all the probe molecules present in **2**/$CaCl_2$ gels. The dashed line is the spectrum when an exponential line broadening factor of 4 Hz is applied to the FID prior to Fourier transformation. (Bottom) ^{43}Ca NMR spectrum of a **2**/$CaCl_2$ gel. The concentration of free Ca^{2+} ions was uniform throughout the sample at 25±6 mM.

No ^{43}Ca NMR resonances are apparent in a **2**/$CaCl_2$ gel whereas a sharp peak is observed in an analogous solution at the same pH in the absence of **2**. We can thus invoke the existence of a fast exchange of the Ca^{2+} ions between the gel fibres and the solution phase that broadens the ^{43}Ca resonance to the extent that it is not visible above the baseline noise. We can estimate a lower limit for the fraction of Ca^{2+} ions, $f_{b,min}$, that are associated with the gel fibres at any instant. Assuming a Lorentzian line shape, the observed ^{43}Ca half-height line width, w_{obs}, in the gel is given by:

$$w_{obs} = f_b w_b + (1 - f_b) w_f \qquad \text{(S11.1)}$$

where w_{obs} and w_f are the ^{43}Ca line widths of the Ca^{2+} ions associated with the fibres and free in solution respectively. f_b is the fraction of Ca^{2+} ions associated with the gel fibres. Rearranging S11.1:

$$f_b = \frac{}{w_b - w_f} \qquad \text{(S11.2)}$$

The minimum linewidth, w_{min}, for a resonance to be visible above the baseline noise is given by:

$$w_{min} = \frac{}{h_n} \qquad \text{(S11.3)}$$

where h_n and h_f are respectively the heights of the noise and the ^{43}Ca resonance in the solution in the absence of **2**. From Figure S11, h_f/h_n = 4 and w_f = 1 Hz, and it can thus be estimated that a resonance with a width greater than 4 Hz would not be observable. This theory is confirmed by

applying an artificial broadening factor of 4 Hz to the spectrum (Figure S11, dashed line) – the peak is at the same level as the noise when no line broadening factor is applied. Combining S11.2 and S11.3:

$$f_{b,min} = \frac{w_f\left(\overline{h_n}^{-1}\right)}{w_b - w_f} \qquad \text{(S11.4)}$$

A sensible estimate for w_b is 200 Hz, based on the ^{43}Ca linewidths of Ca^{2+} bound to Lactalbumins reported by Aramini *et al*.[37] and so $f_{b,min} \geq 1\%$. We note that the non-appearance of a ^{43}Ca-NMR peak in the gel could be attributed to other causes, such as the presence of ^{43}Ca RQCs or a slow exchange of the free and bound Ca^{2+} leading to coalescence of the two resonances. Whatever the cause, a significant interaction of the 'free' Ca^{2+} ions with the gel fibres can be invoked. Spectra were acquired using the aring sequence with a 58 μs pulse (π/2), a sweep width of 2000 Hz, a signal acquisition time of 1 s and a relaxation delay of 0.1 s. 184,000 and 524,000 scans were acquired for the top and bottom spectra of Figure S11 respectively, giving total acquisition times of 2 days 13 hours and 7 days respectively.

12. Stability of a **2**/$CaCl_2$ gel when exposed to an external NaCl solution

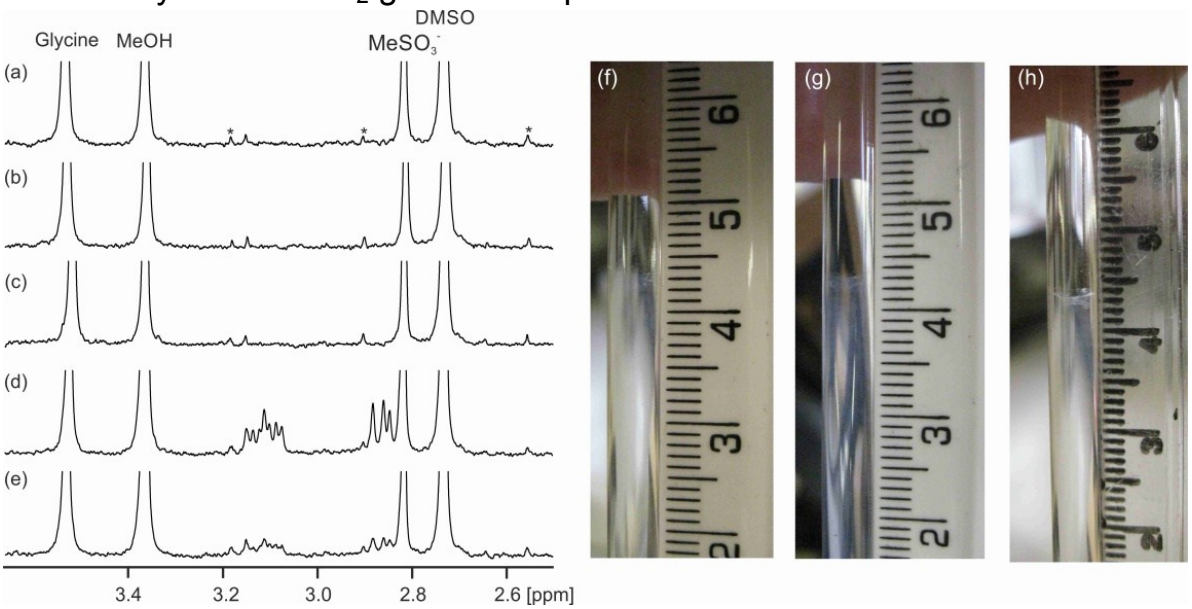

Figure S12. (a-c) ^{1}H NMR spectra of solutions that had stood on top of a **2**/$CaCl_2$ gel: (a) first solution after 26 days, (b) second solution after 9 days and (c) third solution after 17 days. $[Ca^{2+}]_{free}$ in these solutions was measured as 4±1 mM, 1±0.3 mM and < 1 mM respectively. The peaks marked * are ^{13}C satellite peaks of the organic solvents. The satellite to the left of $MeSO_3^-$ (^{13}C-DMSO) corresponds to 40 μM of ^{1}H nuclei. (d) ^{1}H NMR spectrum of solution of **2** at a concentration 0.4 mg/mL. (e) Sample of (d) after addition of 1 mM $CaCl_2$. Photographs of the top of the gel immediately after the first solution was placed on top (f), after the second solution had stood for 9 days (g) and after the third solution had stood for 17 days (h). The ruler was held against the bottom of the tube in all images.

No resonances attributable to **2** were detectable in the solutions that had stood on top of the gels (a-c). An 0.4 mg/mL solution of **2** is shown for comparison (d) where the resonances of the CH_2 protons of the phenylalanine are clearly visible. Addition of 1 mM $CaCl_2$ to the 0.4 mg/mL solution of **2** resulted in a white precipitate, suggesting a very low solubility of **2** in the presence of Ca^{2+} (e). No swelling or erosion of the gels was visually apparent at any stage (f-h). When the third solution was removed from the gel (c and h), $[Ca^{2+}]_{free}$ in the gel had dropped to 4±1 mM. Spectra were acquired using a double-echo WATERGATE sequence in 8 scans with a signal acquisition time of 3.7 s and a relaxation delay of 1 s.

13. ^{23}Na and ^{2}H analysis of **2**/$CaCl_2$ gel exposed to external NaCl solutions

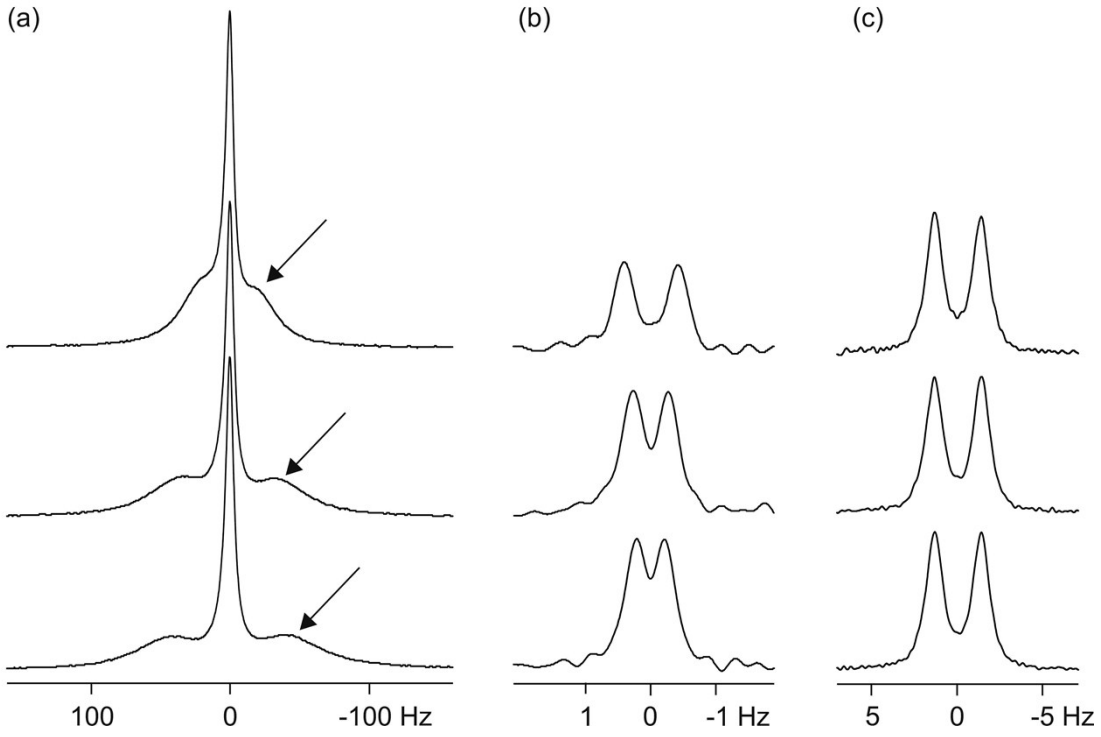

Figure S13. NMR spectra of $^{23}Na^{+}$ (a), sodium formate-d (b) and dioxane-d_8 (c) in **2**/$CaCl_2$ gel of Figure 6 before an NaCl solution was placed on top (upper), at the end of the second series of measurements (middle) and after a third solution had stood on top of gel for 17 days (lower). Although $^{23}Na^{+}$ RQCs cannot be resolved, the 'satellite' peaks (arrowed) move away from the central resonance indicating a stronger interaction of Na^{+} with the fibres.

14. Quantification of the amount of negative charge on **3**/DMSO gels

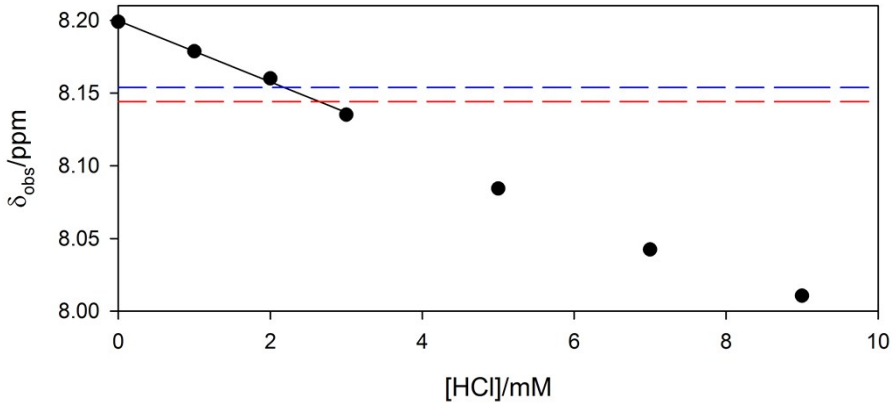

Figure S14a. Plot of formate chemical shift, δ_{obs}, versus concentration of HCl. The solid black line is a fit to Equation S14. The dashed lines represent the chemical shifts of formate in two nominally identical **3**/DMSO gels prepared using the standard set of probe molecules listed in the text.

Solutions of the probe molecules, detailed in the main text, were prepared in 80% H_2O, 20% DMSO at different concentrations of HCl. From Figure S14, it is apparent that the formate resonance in 5 mg/mL (12 mM) gels of **3** is shifted by the same amount as when 2.4±0.2 mM HCl is included in the absence of **3** (data from two samples). HCl behaves as a strong acid even in DMSO[38] and so 2.4±0.2 mM H^+ has been transferred to the formate from **3**. The fraction of carboxylates of **3** in the gel samples that are deprotonated can thus be calculated as (2.4±0.2)/12 = 20±2%. When the concentration of HCl is less than the total concentration of formate, $[Form]_{tot}$, the concentration of formic acid in the sample will be equal to the concentration of added HCl, the concentration of free H^+ being negligible. The observed chemical shift of formate, δ_{obs}, is thus described by the equation:

$$\delta_{obs} = \delta_l - [HCl]\frac{\upsilon_l - \upsilon_H}{[Form]_{total}} \qquad \text{(S14)}$$

where δ_l and δ_H are the limiting chemical shifts of formate in the fully deprotonated and protonated states. $[Form]_{total}$ is the total concentration of formate and formic acid. This equation provides an acceptable fit between 0 and 3 mM HCl (Figure S14a). To investigate the effect of hydrogen bonding to the gel fibres of **3** on the formate chemical shifts, a solution of the probe molecules was prepared and the pH adjusted to 4.5 with HCl; the same pH as the **3**/DMSO gel containing the probe molecules. The chemical shift of formate in this sample was measured as 8.153 ppm, in very close agreement with the shift measured in a **3**/DMSO gel. We can conclude that any H-bonding of formate to the gel fibres does not significantly affect its chemical shift.

pH measurements were performed using a Hanna Instruments 'Edge' pH data logger equipped with an FC2020 probe. Before use, the meter was calibrated using fresh pH 4, 7, and 10 buffer solutions. The pH of 1 mM HCl was measured as 3.06 in H_2O and 3.15 in 80% H_2O, 20% DMSO and was unaffected by the addition of 15 mM NaCl. Our meter is thus only slightly (< 0.1 pH unit) affected by the presence of the DMSO.[39] Self-supporting hydrogels were formed with either pure H_2O or with the standard set of probe molecules listed in the main text (Figure S14b).

Figure S14b. Photographs of **3**/DMSO gels prepared with the set of probe molecules listed in the text (left) or with pure H_2O (right), 20 hours after preparation.

15. ^{1}H NMR analysis of **3**/DMSO gels

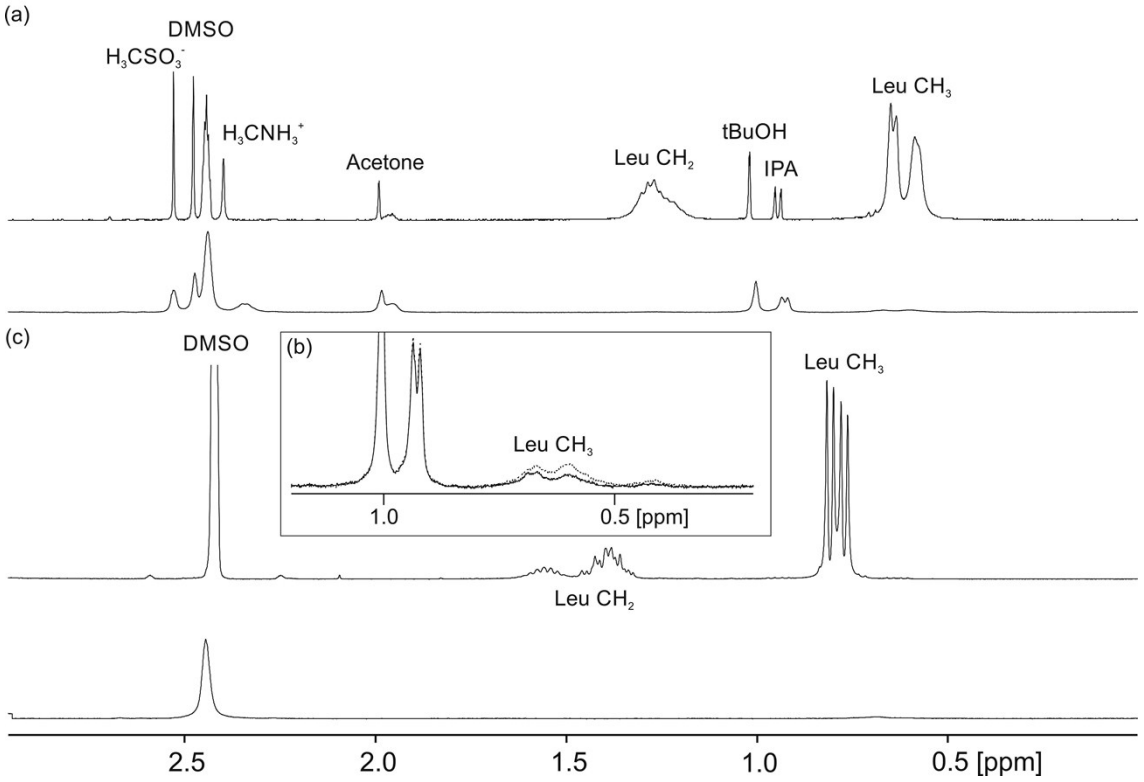

Figure S15a. (a) ^{1}H NMR spectrum of **3**/DMSO gel sample as prepared at 298 K (lower plot) and when heated to 363 K (upper plot) to melt the sample.[27] This gel contained the probe molecules listed in the text. The spectra have been scaled according to the absolute integrals of the DMSO, methylammonium and methanesulfonate peaks and referenced to methanesulfonate (2.53 ppm). By integration, less than 5% of **3** is visible in the gel as prepared at 298 K, as compared to 363 K. (b) (inset) Expanded spectrum of **3**/DMSO gel at 298 K recorded with (solid) and without (dashed) on resonance presaturation applied to the gel fibres. Strong STDs are observed to the signal of the residual gelator indicating a strong interaction/exchange with the self-assembled fibres. (c) ^{1}H NMR spectrum of **3**/DMSO gel without any probe molecules as prepared at 298 K (lower plot) and 5 mg/mL **3** dissolved in 100% DMSO-d_6 (upper plot). The spectra have been scaled according to the absolute integral of the residual protonated peak of the DMSO-d_6. Again, less than 5% of **3** is visible in the gelled state at 298 K. The peaks in the gels at 298 K are broad due to entrapped air bubbles. Spectra shown were obtained using the standard sequence for STD measurements with off-resonance presaturation. Analogous results were obtained with no presaturation applied.

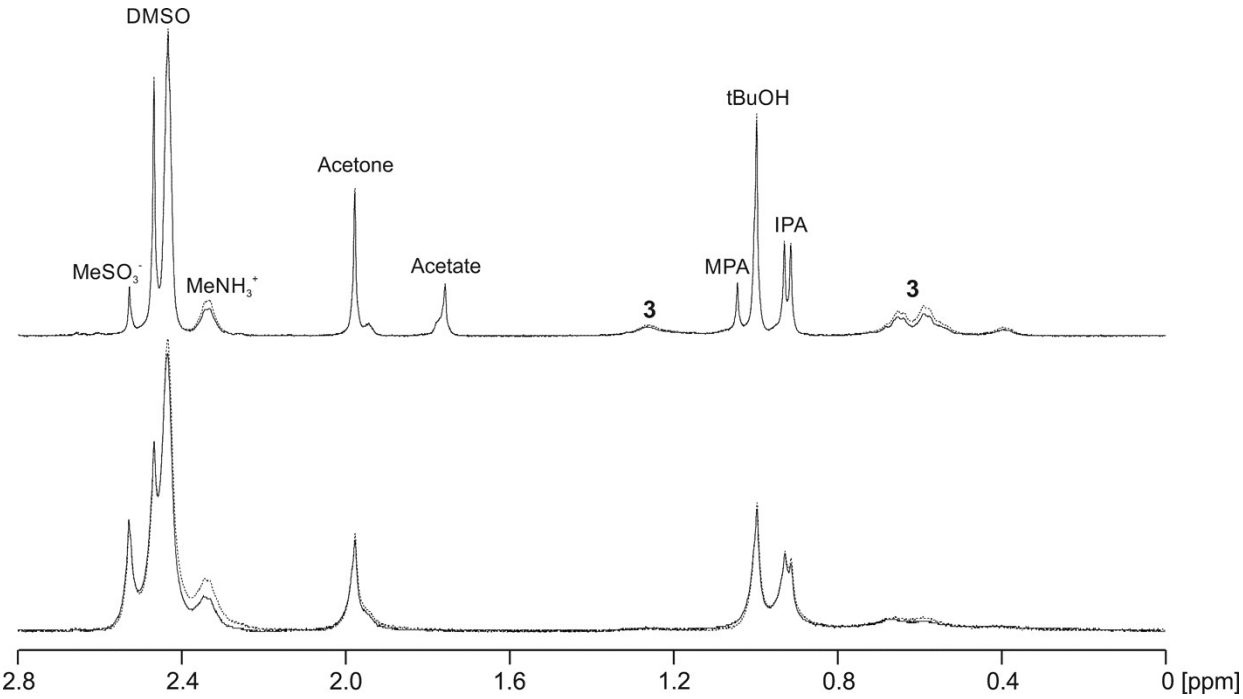

Figure S15b. ^{1}H NMR spectra of **3**/DMSO gels recorded with (solid) or without (dashed) on-resonance presaturation applied to the gel fibres. Gels were prepared with the standard set of probe molecules listed in the main text (lower) or with 1 mM glycinate, MPA^{2-}, acetate, 2 mM formate-h, 5 mM formate-d, 0.5 mM methanesulfonate and all of the ^{1}H and ^{2}H solvents listed in Table 1 at 0.05 and 0.01 vol% respectively (upper). Methanol-d_3 was included at 0.02 vol%. Spectra were recorded 20 minutes after gel preparation. The lower spectra have been scaled to the same height as the upper spectra to balance the effect of the broader lines (greater air-bubble formation) in the lower sample. The ^{1}H NMR resonances of **3** are larger when the basic additives are included (Figure S15b).

16. Comparison of ^{1}H gelator integrals of **1** during formation of **1**/GdL gels acquired with presaturation and WATERGATE solvent suppression techniques

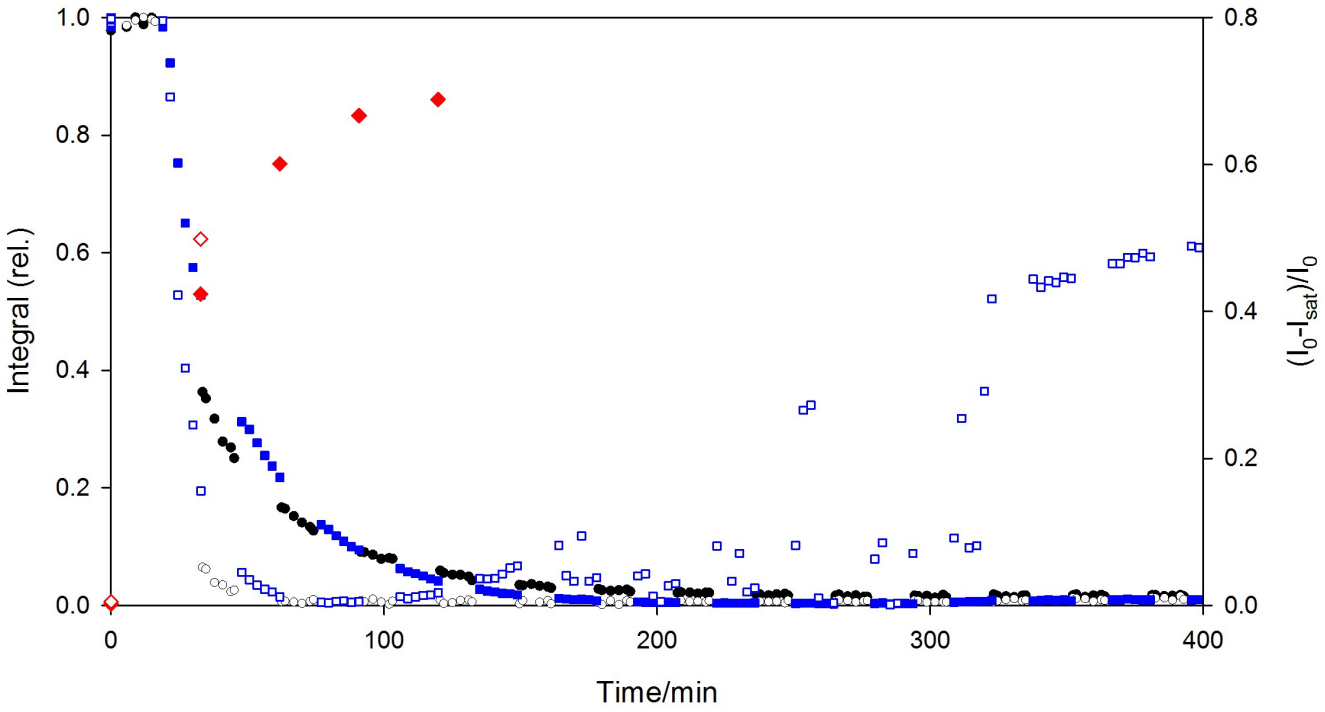

Figure S16. Plots of ^{1}H integrals of valine methyl (solid symbols) and aromatic (hollow symbols) resonances of **1** during formation of **1**/GdL gel. Integrals were obtained either in a single scan with presaturation applied to the H_2O resonance (black circle) or using a double-echo WATGERGATE sequence (blue square). WATERGATE integrals were obtained from off-resonance STD spectra. STDs (8 s presaturation time) to the gelator resonances (red diamond) are also plotted. After 100 minutes, NH resonances of NH_4^+ and $MeNH_3^+$ become visible on WATERGATE spectra that overlap with the aromatic region of the gelator integral.

Integrals acquired using either presaturation or WATERGATE solvent suppression techniques are qualitatively the same, although we note that neither method is strictly quantitative. Spectra recorded with presaturation to H_2O are affected by STDs to the NMR-visible gelators while WATERGATE spectra are affected by T_2 relaxation during the pulse sequence and J-modulation effects. No STDs are apparent to the gelators before the addition of GdL, indicating minimal aggregation of the gelators at high pH. Upon assembly, strong STDs become apparent to both resonances of the gelator indicating a strong interaction or exchange of the NMR-visible gelator with the newly-formed fibres. We note that the STD spectra were acquired with interleaved on and off-resonance scans, each of 10 s, and so assembly of the gelators during an individual STD measurement will not significantly affect the results. The faster disappearance of the aromatic resonance of **1** can be attributed to a stronger affinity of this hydrophobic portion of the molecule for **1**/GdL fibres relative to the dipeptide portion of the molecule. Analogous results were obtained for **3**/GdL gels (data not shown).

References

1. M. Wallace, J. A. Iggo and D. J. Adams, *Soft Matter*, 2015, **11**, 7739-7747.
2. Y. Pocker and E. Green, *J. Am. Chem. Soc.*, 1973, **95**, 113-119.
3. M. Tena-Solsona, B. Escuder and J. F. Miravet, *Chem. Mater.*, 2015, **27**, 3358-3365.
4. A. Z. Cardoso, L. L. E. Mears, B. N. Cattoz, P. C. Griffiths, R. Schweins and D. J. Adams, *Soft Matter*, 2016, **12**, 3612-3621.
5. J. Kříž and J. Dybal, *J. Phys. Chem. B*, 2004, **108**, 9306-9314.
6. M. M. Chui, R. J. Phillips and M. J. McCarthy, *J. Colloid Interface Sci.*, 1995, **174**, 336-344.
7. J. J. H. Ackerman, G. E. Soto, W. M. Spees, Z. Zhu and J. L. Evelhoch, *Magn. Reson. Med.*, 1996, **36**, 674-683.
8. C. A. Lepre, J. M. Moore and J. W. Peng, *Chem. Rev.*, 2004, **104**, 3641-3675.
9. J. Angulo, P. M. Enríquez-Navas and P. M. Nieto, *Chem. Eur. J.*, 2010, **16**, 7803-7812.
10. A. Delville, J. Grandjean and P. Laszlo, *J. Phys. Chem.*, 1991, **95**, 1383-1392.
11. D. T. Edmonds and A. L. Mackay, *J. Magn. Reson.*, 1975, **20**, 515-519.
12. B. Halle and H. Wennerström, *J. Chem. Phys.*, 1981, **75**, 1928-1943.
13. P. Porion, M. P. Faugère, E. Lécolier, B. Gherardi and A. Delville, *J. Phys. Chem. B*, 1998, **102**, 3477-3485.
14. M. Wallace, A. Z. Cardoso, W. J. Frith, J. A. Iggo and D. J. Adams, *Chem. Eur. J.*, 2014, **20**, 16484-16487.
15. C. Naumann, W. A. Bubb, B. E. Chapman and P. W. Kuchel, *J. Am. Chem. Soc.*, 2007, **129**, 5340-5341.
16. A. Canales, J. Jiménez-Barbero and M. Martín-Pastor, *Magn. Reson. Chem.*, 2012, **50 Suppl 1**, S80-S85.
17. D. E. Woessner, *Concepts Magn. Reson.*, 2001, **13**, 294-325.
18. L. A. Rijniers, P. C. M. M. Magusin, H. P. Huinink, L. Pel and K. Kopinga, *J. Magn. Reson.*, 2004, **167**, 25-30.
19. W. H. Braunlin, H. J. Vogel and S. ForsÉN, *Eur. J. Biochem.*, 1984, **142**, 139-144.
20. H. Gustavsson and B. Lindman, *J. Am. Chem. Soc.*, 1975, **97**, 3923-3930.
21. A. Castilla, M. Wallace, l. Mears, E. Draper, J. Doutch, S. E. Rogers and D. J. Adams, *Soft Matter*, 2016, **12**, 7848-7854.
22. E. R. Draper, J. R. Lee, M. Wallace, F. Jackel, A. J. Cowan and D. J. Adams, *Chem. Sci.*, 2016, **7**, 6499-6505.
23. M. D. Segarra-Maset, B. Escuder and J. F. Miravet, *Chem. Eur. J.*, 2015, **21**, 13925-13929.
24. A. Pallagi, P. Sebk, P. Forgó, T. Jakusch, I. Pálinkó and P. Sipos, *Carbohydr. Res.*, 2010, **345**, 1856-1864.
25. A. Z. Cardoso, A. E. Alvarez Alvarez, B. N. Cattoz, P. C. Griffiths, S. M. King, W. J. Frith and D. J. Adams, *Faraday Discuss.*, 2013, **166**, 101-116.
26. N. A. Dudukovic and C. F. Zukoski, *Langmuir*, 2014, **30**, 4493-4500.
27. L. Chen, J. Raeburn, S. Sutton, D. G. Spiller, J. Williams, J. S. Sharp, P. C. Griffiths, R. K. Heenan, S. M. King, A. Paul, S. Furzeland, D. Atkins and D. J. Adams, *Soft Matter*, 2011, **7**, 9721-9727.
28. A. Rapp, K. Ermolaev and B. M. Fung, *J. Phys. Chem. B*, 1999, **103**, 1705-1711.
29. P. Van Der Asdonk, M. Keshavarz, P. C. M. Christianen and P. H. J. Kouwer, *Soft Matter*, 2016, **12**, 6518-6525.
30. B. Escuder, J. F. Miravet and J. A. Sáez, *Org. Biomol. Chem.*, 2008, **6**, 4378-4383.
31. J. A. Sáez, B. Escuder and J. F. Miravet, *Chem. Commun.*, 2010, **46**, 7996-7998.
32. A. de Robertis, S. Sammartano and C. Rigano, *Thermochim. Acta*, 1984, **74**, 343-355.
33. D. A. Palmer and R. Van Eldik, *Chem. Rev.*, 1983, **83**, 651-731.
34. P. G. Daniele, A. De Robertis, C. De Stefano, S. Sammartano and C. Rigano, *J. Chem. Soc., Dalton Trans.*, 1985, 2353-2361.
35. D. J. Miller, *Colloid Polym. Sci.*, 1989, **267**, 929-934.

36. H. Shinar and G. Navon, *Biophys. J.*, 1991, **59**, 203-208.
37. J. M. Aramini, T. Drakenberg, T. Hiraoki, Y. Ke, K. Nitta and H. J. Vogel, *Biochemistry*, 1992, **31**, 6761-6768.
38. A. Trummal, L. Lipping, I. Kaljurand, I. A. Koppel and I. Leito, *J. Phys. Chem. A*, 2016, **120**, 3663-3669.
39. P. Mukerjee and J. D. Ostrow, *Tetrahedron Lett.*, 1998, **39**, 423-426.